

AHC: An integrated numerical model for simulating agroecosystem processes—Model description and application

Xu Xu^{a,b}, Chen Sun^c, Fengtian Neng^{a,b}, Jing Fu^{a,b}, Guanhua Huang^{a,b,*}

^a Chinese-Israeli International Center for Research and Training in Agriculture, China Agricultural University, Beijing 100083, PR China

^b Center for Agricultural Water Research, China Agricultural University, Beijing 100083, PR China

^c Institute of Environment and Sustainable Development in Agriculture, Chinese Academy of Agricultural Sciences, Beijing 100081, PR China

ARTICLE INFO

Keywords:
Soil water
Salinity
Nitrogen
Crop growth
Model calibration
Numerical modeling

ABSTRACT

This article introduces the AHC model as a new tool for modeling and assessing the agroecosystem processes. The AHC, as a one-dimensional numerical physical model, simulates the soil water and salt/nitrogen dynamics, heat transport, and crop growth and yield in various soil-crop environments. The key features of the AHC include that it provides the optional function for simulating the fate of salt or nitrogen; it has an efficient global method for sensitivity analysis and parameter estimation; and it is useful in a wide range of field conditions, especially for those in northern China. A menu-driven program is developed as a user-friendly interface for efficient data manipulation. This paper primarily describes the main structures and algorithms of the AHC and presents its field applicability. Model testing and application was conducted with two cases: (1) a salinity case with maize growing in salt-affected fields under arid and shallow groundwater environments (Hetao, upper Yellow River basin, northwest China); and (2) a nitrogen case with a wheat-maize rotation system in the semihumid monsoon region (Tai'an, North China Plain). Good agreement was obtained between the simulated and observed data, including the soil water contents, salt/nitrogen contents, and crop growth indicators. The soil water and salt/nitrogen dynamics, crop growth processes, and their complex interactive effects were also well interpreted using the AHC. Rational simulation proves the good applicability of the AHC for practical field use.

1. Introduction

Agroecosystem models can be defined as a quantitative scheme for predicting hydrological, chemical and biological processes in soil-crop systems, with relevant human and environmental factors on various scales (Monteith, 1996; Sinclair and Seligman, 2000; Steduto et al., 2009). The functions and applications of the model mainly include evaluating field experiments, searching for the best management practices, and use as heuristic tools in teaching and research (Sinclair and Seligman, 1996; Cameira et al., 2007; Šimůnek et al., 2016). Current agroecosystem models have varying degrees of numerical sophistication, ranging from purely empirical to highly mechanistic (Monteith, 1996; Kucharik, 2003). In the aspect of agro-hydrological processes, the models can be classified as balance and physically mechanistic models. The former includes the lumped balance models (e.g., SIMDualKc) and the cascading layer models (e.g., AquaCrop and DSSAT) (Rosa et al., 2012; Steduto et al., 2009; Jones et al., 2003). The latter are fully based on deterministic and physical laws, such as

HYDRUS, SWAP, Daisy and RZWQM (Šimůnek et al., 2005; van Dam et al., 1997; Hansen, 2002; Ahuja et al., 2000). For the aspect of crop growth and yield formation, the models might be divided into empirical models and process-based models. Empirical models consist of empirical functions that are chosen to fit measurements from the field. Process-based models often simulate the plant biomass or organ development based on the plant physiology or morphology, typically as EPIC, WOFOST and DSSAT (Williams et al., 1984; van Diepen et al., 1989; Hoogenboom et al., 2015). So far, agro-ecosystem modeling is still facing some disputes and dilemmas in the generality of models and in the balance of simplicity and complexity (Therond et al., 2011; Rosa et al., 2012; Sinclair and Seligman, 2000).

On the other hand, existing agroecosystem models generally have different functionalities for practical use. Models for irrigation management mainly focus on soil water, salinity and crops (e.g., SIMDualKc, AquaCrop, SWAP and SaltMod (Oosterbaan, 2001)), while the suite of specialized crop models always includes the simulation of the fate of nutrients or even the soil carbon balance, such as EPIC,

* Corresponding author at: Chinese-Israeli International Center for Research and Training in Agriculture, China Agricultural University, Beijing 100083, PR China.

E-mail addresses: xushengwu@cau.edu.cn, xuxu23@qq.com (X. Xu), sunchen621@foxmail.com (C. Sun), nengft@cau.edu.cn (F. Neng), fuj1219@cau.edu.cn (J. Fu), ghuang@cau.edu.cn (G. Huang).

RZWQM, DSSAT and APSIM (McCown et al., 1996). Moreover, some researchers conclude that the agroecosystem models can be classified into two types of approaches: scientific and engineering (Steduto et al., 2009). The first aims to improve the understanding of crop behavior based on physiology, and the second attempts to provide management advice to farmers and policymakers. Generally, a common consensus is that it is impossible to create universal models, as each season or new location brings new challenges that are not foreseen in the original model (Sinclair and Seligman, 2000). Therefore, considerable and continuous efforts of modification of model functions are thus necessary to make the model cope with discrepancies that derive from the changes in the peculiarities of the application environments (Sinclair and Seligman, 1996, 2000; Coucheney et al., 2015; Xu et al., 2016).

Model calibration is another major challenge in agroecosystem modeling, involving a sensitivity analysis (SA), parameter estimation (PE) and uncertainty analysis (Xu et al., 2016). The SA is a critical step to identify the sensitive and important parameters (DeJonge et al., 2012). The most popular SA practice is that of the OAT (One-factor-At-a-Time) method, which has the limitation of local attributes of data sampling. In addition to local methods, global sensitivity analysis (GSA) methods are recently more preferred and applied to some agroecosystem models, typically as the extended FAST, Sobol' and LH-OAT methods (Zhao et al., 2014; Della Peruta et al., 2014; Xu et al., 2016). The automatic inverse optimization method is becoming a preferred alternative in parameter estimation. The local PE method has been widely used; however, it may prematurely terminate the search and thus is prone to find local rather than global minima (Šimůnek et al., 2012). The global PE methods become a better alternative when more parameters are to be estimated or a more complex model adopted. Some classic applications in agroecosystem modeling include the use of PEST, genetic algorithm, GLUE, Ensemble Kalman Filter and shuffled complex methods (Doherty, 2005; Ines and Droogers, 2002; Abbaspour et al., 2001; Evensen, 2003; Duan et al., 1994). To our knowledge, only a few mature models release their own specific PE module for practical use, e.g., the inverse solution based on the gradient-type minimization method in HYDRUS-1D (Šimůnek et al., 2012) and the DSSAT GLUE program (Jones et al., 2011). An uncertainty analysis is also applied for model parameters (Xu et al., 2016), however, especially in watershed hydrologic modeling because of the high uncertainty at large scales (Yang et al., 2008).

In view of previous studies, the agroecosystem models developed by different research institutions usually have relatively specific backgrounds, features and adaptabilities. The deficiencies in the application of existing models may be considered as: (1) most models only focus on either the salinity simulation or the nitrogen simulation and the interaction with crop growth; (2) few models provide mature functions to efficiently handle the parameter calibration; and (3) the models often cannot be directly used in changed environments (different from its original development) without a certain or even significant degree of modification of model functions. Meanwhile, the water deficit, secondary salinity and unreasonable nitrogen fertilization are the three most significant issues that agroecosystems are facing in many regions worldwide. These issues exist particularly in different areas of northern China. Therefore, in this paper, we propose a new model/software (named AHC) for agroecosystem simulation, with the motivation of integrating our previous experimental and modeling work related to various conditions in the Yellow River basin, North China Plain and Hexi Corridor region of northern China (Xu et al., 2011, 2012a; Xu et al., 2012b, 2013; Xu et al., 2015, 2016; Jiang et al., 2015; Wang and Huang, 2008; Wang et al., 2015; Ren et al., 2016; Neng, 2016). The AHC is developed as a systematic tool to numerically simulate the soil water flow, the fate of salt or nitrogen, heat transport, and crop growth and yield with the effects of ambient environmental changes. The efficient global methods for sensitivity analysis and inverse estimation of parameters are also involved. The conceptual framework and distinctive components and features of the AHC are herein described, and

then the model is applied in two case studies related to salinity and nitrogen issues, respectively. These two examples of applications could provide a comprehensive presentation of the main features and applicability of our proposed model.

2. Model description

2.1. Overview of AHC and its components

The AHC (Agro-Hydrological & chemical and Crop systems simulator) is designed with two main parts, i.e., the mathematical model and the graphical user interface (GUI). The mathematical model as the core of the AHC could be seen as composed of three processes: Agroecosystem-Simulation (AESIM) Process, Global-Sensitivity-Analysis (GSA) Process, and Global-Parameter-Estimation (GPE) Process. Process could be defined as a kind of modularization entity, and each process is a part of code that performs certain functions by specific methods. The source code is all written in FORTRAN and compiled with Intel Visual Fortran Composer XE 2011. The friendly GUI is developed for pre- and post-processing of datasets using the Visual Basic.NET (VB.NET) programming language in Microsoft Visual Studio 2010. The mathematical model of FORTRAN codes is packaged into the GUI program.

The AESIM Process is inherited and modified from the previous agro-hydrological model SWAP-EPIC. It consisted of five main modules related to soil water, evaporation and transpiration, solute, heat and plant. The main calculation flow chart is presented in Fig. 1. The soil water module is mainly drawn from the SWAP model (van Dam et al., 1997), with significant improvements related to soil evaporation, root water uptake, soil thawing, etc. (Xu et al., 2013, 2015). The solute transport module was originally developed by Xu et al. (2016) for the simulation of salinity, which is adopted and continuously improved. In particular, the function of simulating the fate of nitrogen is newly added for solute transport in AHC, which is based on the previous modeling work on nitrogen simulation on the North China Plain (NCP) (Wang and Huang, 2008; Wang et al., 2015; Liang et al., 2014). The heat transport is simulated using a convection-dispersion equation. Crop growth and yield formation are simulated with the modified EPIC crop growth model (Williams et al., 1989), with the code compiled by Xu et al. (2013). Thus, the AHC became a one-dimensional (1-D) physically-based model that, in brief, simulates water flow, solute transport and transformation (optionally salt or nitrogen), heat transport, and crop growth and yield in agricultural fields. The simulation of soil water, salt and crop growth has been preliminarily tested with several crops (e.g., wheat, maize, cabbage and sunflower) and different field conditions (e.g., different soils and deep or shallow water tables) when using the previous version SWAP-EPIC (Xu et al., 2013; Jiang et al., 2015; Xu et al., 2015; Neng, 2016). By close coupling with ArcInfo 9, the GIS-based version is also applied to access the regional water use and water productivity (Xu et al., 2011; Jiang et al., 2015).

The GSA Process and GPE Process are used in conjunction to determine the parameters for model calibration. The former is based on an efficient Latin Hypercube One-factor-At-a-Time (LH-OAT) method, and the latter is developed using the modified Micro Genetic Algorithm (modified-MGA). They have been developed and preliminarily tested in the parameter calibration of SWAP-EPIC, with a two-year experiment in a salt-affected wheat field (Xu et al., 2016). The friendly GUI is preliminarily developed by Neng (2016), with continuous testing and improvement.

2.2. Detailed description of model components and mechanisms

2.2.1. Agroecosystem-Simulation (AESIM) Process

(1) Soil water flow

The soil water flow module is based on using the 1-D Richards' equation for vertical flow:

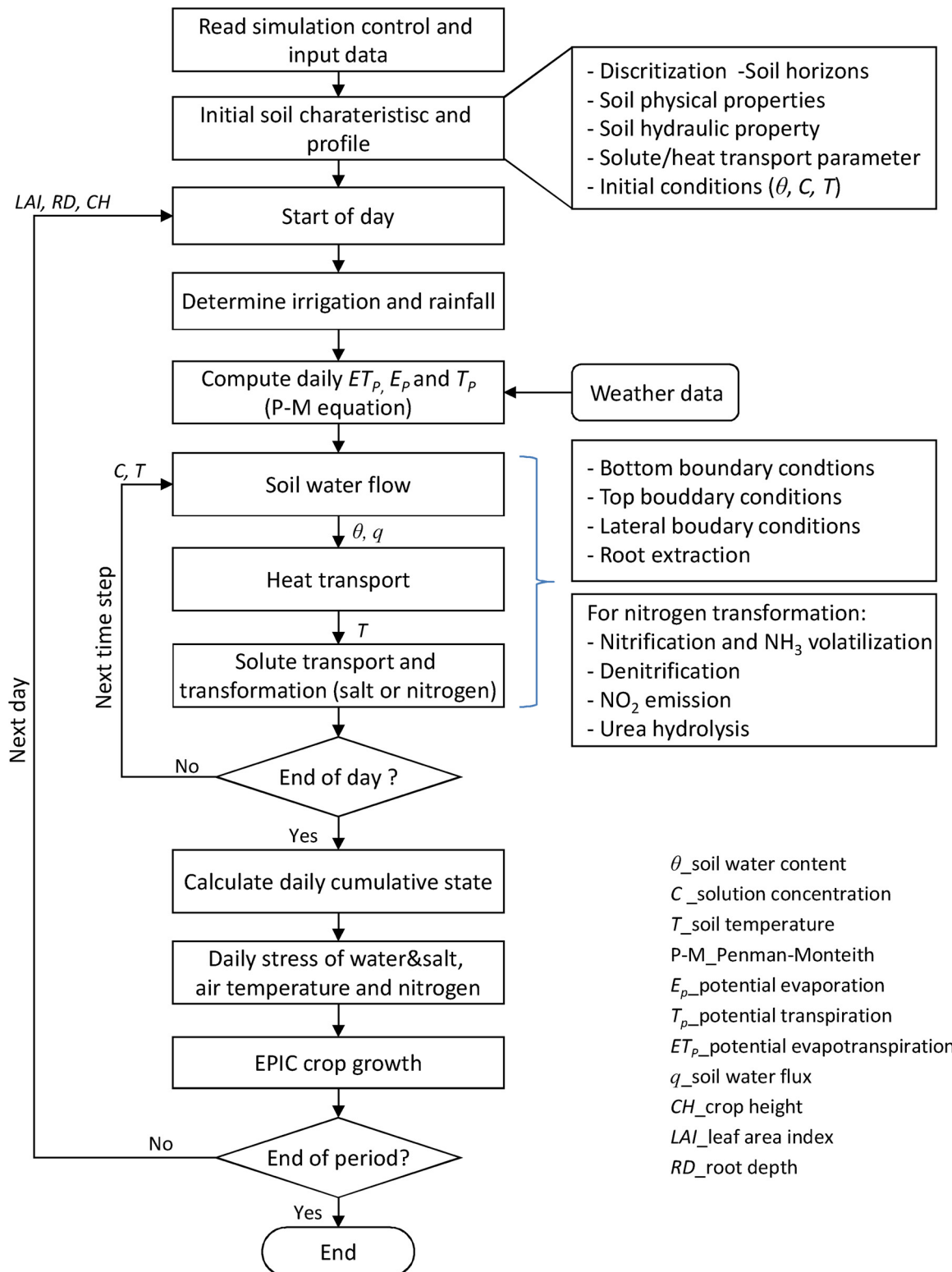


Fig. 1. The calculation procedure of the Agroecosystem-Simulation (AESIM) Process in AHC.

$$C(h) \frac{\partial h}{\partial t} = \frac{\partial}{\partial z} \left[K(h) \left(\frac{\partial h}{\partial z} + 1 \right) \right] - S(h) \quad (1)$$

where C is the differential soil water capacity (cm^{-1}), h is the soil water pressure head (cm), t is time (d), z is the vertical coordinate (cm, positive upward), K is the hydraulic conductivity (cm d^{-1}) and S is the sink term ($\text{cm}^3 \text{cm}^{-3} \text{d}^{-1}$). This equation is solved using an implicit finite-difference scheme. Eq. (1) requires knowledge of the soil hydraulic

properties, which are described by the van Genuchten-Mualem (VGM) model (van Genuchten, 1980; Mualem, 1976), as follows:

$$S_e(h) = \frac{\theta(h) - \theta_r}{\theta_s - \theta_r} = \frac{1}{(1 + |\alpha h|^n)^{1-1/n}} \quad (2)$$

$$K(h) = K_s S_e^{\lambda} [1 - (1 - S_e^{n/(n-1)})^{1-1/n}]^2 \quad (3)$$

where S_e is the effective saturation, θ is the soil water content

($\text{cm}^3 \text{cm}^{-3}$), θ_r and θ_s denote the residual and saturated water contents ($\text{cm}^3 \text{cm}^{-3}$), respectively, K_s is the saturated hydraulic conductivity (cm d^{-1}), $\alpha (\text{cm}^{-1})$ and $n (-)$ are empirical shape parameters, and λ is a pore connectivity/tortuosity parameter (-).

The top boundary condition can be determined by the rates of actual evaporation (E_a) and actual transpiration (T_a) and the fluxes of irrigation, precipitation and interception. Potential evapotranspiration (ET) is estimated by the Penman-Monteith equation (Monteith, 1965), and it is first separated into potential soil evaporation (E_p) and potential crop transpiration (T_p) based upon the leaf area index (LAI). Actual evaporation and transpiration rates are then respectively obtained as a function of the available soil water in the surface soil and the root zone. Three functions could be optionally used to estimate E_a under dry soil conditions. The effect of film mulches on soil evaporation can be considered to further limit the soil evaporation. Moreover, a “surface reservoir” boundary condition is applied if surface ponding is expected to develop. Additionally, the surface runoff is allowed when the water ponding depth is over a user-specified maximum ponding height. The detailed calculations related to the upper boundary can be found in Annex A.

The model further provides eight options to prescribe the lower boundary conditions: the Dirichlet type (pressure head as a function of time), Neumann type (bottom flux as a function of time), Cauchy type (bottom flux as a function of groundwater level), and free drainage in deep groundwater level conditions. Lateral field drainage fluxes to the drainage system are alternatively simulated using a simple linear or nonlinear (i.e., using the drainage equations of Hooghoudt and Ernst) relationship between groundwater level and drainage flux. Since the treatment of the bottom boundary conditions and lateral drainage is kept same as that in SWAP model, a brief introduction of principles and equations is provided in Annex E. A more detailed description can be found in Kroes and van Dam (2003). Initial conditions can be implemented with three input options: the soil water content, pressure heads, or a groundwater level when assuming hydrostatic equilibrium in the soil profile.

The sink term, S , is the actual soil water extraction rate by plant roots. Its potential rate at a certain depth $S_p(z)$ is calculated by distributing T_p into each root zone compartment, as a function of the specified root length density. The actual root water uptake rate $S_a(z)$ is determined by considering the water and salt stress that is assumed to be multiplicative. The integration of $S_a(z)$ over the rooting depth is equal to the T_a rate. In addition, the function of the compensated root water uptake could be considered following the conception of Jarvis (1989). It represents a threshold value, above which the root water uptake reduced in stressed parts of the root zone is fully compensated by uptake from other, less-stressed parts (Šimůnek and Hopmans, 2009). The detailed algorithm for root water uptake under stress can be found in Annex A.

(2) Solute transport and transformation: salinity and nitrogen

A significant modification is introduced to the solute module for the AHC compared with the older version of SWAP-EPIC (only for salinity issue) in Xu et al. (2016). In the latest module, the general formulation of the mass conservation and transport equations involving in a sequential first-order decay chain during transient water flow in a variably saturated rigid porous medium are taken as:

$$\begin{aligned} \frac{\partial(\theta c_1 + \rho_b Q_1)}{\partial t} = & -\frac{\partial q c_1}{\partial z} + \frac{\partial}{\partial z} \left[\theta (D_{\text{dif},1} + D_{\text{dis},1}) \frac{\partial c_1}{\partial z} \right] - (\mu_{w,1} + \mu'_{w,1}) \theta c_1 \\ & - (\mu_{s,1} + \mu'_{s,1}) \rho_b Q_1 \\ & - K_{r,1} S c_1 (k=1) \end{aligned} \quad (4)$$

$$\begin{aligned} \frac{\partial(\theta c_k + \rho_b Q_k)}{\partial t} = & -\frac{\partial q c_k}{\partial z} + \frac{\partial}{\partial z} \left[\theta (D_{\text{dif},k} + D_{\text{dis},k}) \frac{\partial c_k}{\partial z} \right] - (\mu_{w,k} + \mu'_{w,k}) \theta c_k \\ & - (\mu_{s,k} + \mu'_{s,k}) \rho_b Q_k \\ & - K_{r,1} S c_k + \mu'_{w,k-1} \theta c_{k-1} + \mu'_{s,k-1} \rho_b Q_{k-1} (2 \leq k \leq n_s) \end{aligned} \quad (5)$$

where the subscripts w and s refer to liquid and solid phases, respectively, and subscript k represents the k th chain number. c is the solute concentration in the soil liquid phase (g cm^{-3}), ρ_b is the dry soil bulk density (g cm^{-3}), Q is the adsorbed solid concentration (g^{-1}), q is the Darcian velocity (cm d^{-1}), D_{dif} is the diffusion coefficient ($\text{cm}^2 \text{d}^{-1}$), D_{dis} is the dispersion coefficient ($\text{cm}^2 \text{d}^{-1}$), μ is the first-order rate coefficient of transformation (d^{-1}), μ' is the similar first-order rate coefficient of transformation providing connections between individual chain species, and K_r is the root uptake preference factor (-). A K_r value greater than 1.0 represents the occurrence of active root uptake.

The fully implicit or Crank-Nicholson, central finite-difference scheme is applied to solve the Eqs. (4) and (5). Grid Peclet number and Courant number are used together to ensure numerical stability. The third boundary condition is applied for both top and bottom boundaries for solute transport. The drainage/infiltration to/from the ditches is also included in the model. The k should be equal to 1 for salinity simulation, without considering the reaction chain and solid adsorption. For nitrogen simulation, the transformation and transport processes including mineralization-immobilization, solid adsorption, nitrification, denitrification, volatilization, nitrous oxide (N_2O) emission, water uptake (positive and active) and leaching are involved in the chain equations. The urea hydrolysis to ammonia is also considered and described using the first-order kinetics equation. The detailed calculation principles related to nitrogen transformation and plant root uptake can be found in Annex B. The concentration flux boundary conditions (third-type) are provided for both upper and bottom boundaries, which is consistent with the actual field conditions.

Moreover, the AHC provides two specific treatments for applying to the frost conditions. First, a variable active-node method is proposed to describe the simulation zone (i.e., active zone) and simulate the fate of soil water and solute during the soil thawing period in a simple way (Xu et al., 2013). This is particularly designed for the cold early spring season when the upper soil layer fully thaws while the underlying frozen soil layer is in the process of thawing (e.g., for spring wheat growth in northwest China). Second, the $K(h)$ is adjusted under frost conditions, because soil water freezes below a soil temperature of 0°C . A detailed description is provided in Annex C.

(3) Heat transport

Neglecting the effect of water vapor diffusion on transport, the 1-D heat transfer can be described with a convection-dispersion equation of the form in the heat transport module, as follows:

$$C_p(\theta) \frac{\partial T}{\partial t} = \frac{\partial}{\partial z} \left[\lambda(\theta) \frac{\partial T}{\partial z} \right] - C_w q \frac{\partial T}{\partial z} \quad (6)$$

where $C_p(\theta)$ and C_w are the volumetric heat capacity ($\text{J cm}^{-3} \text{^\circ C}^{-1}$) of soil and water, respectively, T is the soil temperature ($^\circ\text{C}$), and $\lambda(\theta)$ is the coefficient of the apparent thermal conductivity of the soil ($\text{J cm}^{-1} \text{^\circ C}^{-1} \text{d}^{-1}$). A fully implicit finite difference scheme is applied to solve Eq. (6). The soil heat capacity and thermal conductivity are calculated from the soil composition and the volume fractions of air and water for each compartment, referring to the approach of De Vries (1975). At the soil surface, the daily average air temperature and the temperature of irrigation water are used to define the boundary conditions.

(4) Crop growth and yield

The crop growth module in the AHC (called EPIC_CGM) is mainly based on the concept of the EPIC crop growth model (Williams et al., 1989), also considering the effects of salinity stress and dormancy. This module is developed because its biological process is relatively simple but well applicable to the field/regional issues compared with some other detailed models. EPIC_CGM considers leaf area development, light interception, and the conversion of intercepted light into biomass and yield together with the effects of temperature, water and salt/nitrogen stress. Biomass is computed from the solar radiation intercepted by the crop leaf area, which is estimated with Beer's law (Monsi and Saeki, 1953). The potential increase in biomass on a given day is

estimated as a function of the plant radiation-use efficiency (RUE) with consideration of environmental stress (e.g., from soil water, salinity or nitrogen, and temperature). The RUE is estimated using the approach proposed by Stockle et al. (1992).

LAI is computed for the various phenological development stages considering heat unit accumulation (Williams et al., 1989). LAI represents the level of canopy cover, and is estimated as a function of heat units, crop stress, and development stages. Crop height is estimated like that in the EPIC model (Williams et al., 1989). The fraction of total biomass partitioned to the root system is 30–50% in seedlings and reduces to 5–20% in mature plants (Jones, 1985). This model decreases the fraction of total biomass in roots (f_{root}) linearly from 0.4 at emergence to 0.2 at maturity, which is similar to the EPIC model (Williams et al., 1989). The root depth generally increases rapidly from planting to a specific maximum depth by early mid-season (Borg and Grimes, 1986). The maximum root depth is required and could be specified according to the field observations or the previous literature. The vertical root distribution in the soil profile is assumed to be a piecewise-linear function of the root depth.

The actual crop yield is calculated using the harvest index concept following the EPIC model procedures (Williams et al., 1989), i.e., as a function of the above ground biomass and environmental stress (from soil temperature, soil salinity, fertilizers, etc.). The detailed calculation of EPIC_CGM can be found in Annex D.

2.2.2. Sensitivity-analysis process

The LH-OAT method is adopted in the AHC to perform the parameter sensitivity analysis. It has a sampling strategy that is a combination of Latin Hypercube (LH) and One-factor-At-a-Time (OAT) sampling, and thus allows performing GSA for a long list of parameters with less computational cost (van Griensven et al., 2006). The calculation procedures are presented in detail in Fig. 2, with the parameter number being equal to M as an example. LH-OAT starts with dividing the parameter range into N intervals, and then taking N LH sampling points for each parameter with each interval to be sampled only once. Then, N parameter groups are randomly generated. After that, each parameter group is varied for M times by changing each of the M parameters one

at a time using the OAT design. Thus, it only requires a total of $N \times (M + 1)$ model runs. A global sensitivity index (i.e., S_p) for the j^{th} parameter (i.e., P), corresponding to a criterion, is calculated by averaging the partial effects ($S_{i,P}$) for all LH points (Eq. 7 and Fig. 2).

$$S_p = \frac{1}{N} \sum_{i=1}^N \left| \frac{M(e_{1,i}, \dots, e_{j,i}(1+f_j), \dots, e_{M,i}) - M(e_{1,i}, \dots, e_{j,i}, \dots, e_{M,i})}{[M(e_{1,i}, \dots, e_{j,i}(1+f_j), \dots, e_{M,i}) + M(e_{1,i}, \dots, e_{j,i}, \dots, e_{M,i})]/2} \right| f_j \quad (7)$$

where $M(\cdot)$ refers to the model functions, $e_{j,i}$ is the value for the j^{th} parameter P at the i^{th} LH point sampling, and f_j is the fraction by which the parameter $e_{j,i}$ is changed (a predefined constant with a default value of 5%). The final global sensitivity value for a parameter could then be estimated by the weighted average of the S_p values under multicriteria conditions. GSA result is obtained according to the S_p value, with the largest value being given the rank of 1 and the smallest value being given a rank equal to the total number of parameters analyzed (Xu et al., 2016).

A total of 316 parameters are involved in the SA database, which could be optionally selected in the analysis. They could be arranged in four main groups: those relative to soil water flow, those related to solute transport and transformation, those related to plant growth, and those describing stress factors of water/salt/nitrogen. Their ranges are required and often determined based on the existing literature. The model outputs could be optionally selected as objective variables, including actual evapotranspiration (ET_a), LAI, bottom flux, dry above-ground biomass (D-AGB), and layer-specific soil moisture and solute concentration/content. The parameters with higher sensitivity and uncertainty would be selected for further calibration. More description about calculation procedures and parameter setting of the GSA Process can be found in Xu et al. (2016).

2.2.3. Parameter-estimation process

The genetic algorithm (GA) is a global and robust method searching for the optimum solution to complex problems using the precept of natural selection (Holland, 1975; Goldberg, 1989). The calculation flow chart of the GA and its coupling with the AESIM Process is shown in Fig. 3. The GA consists of three basic operators of selection, crossover

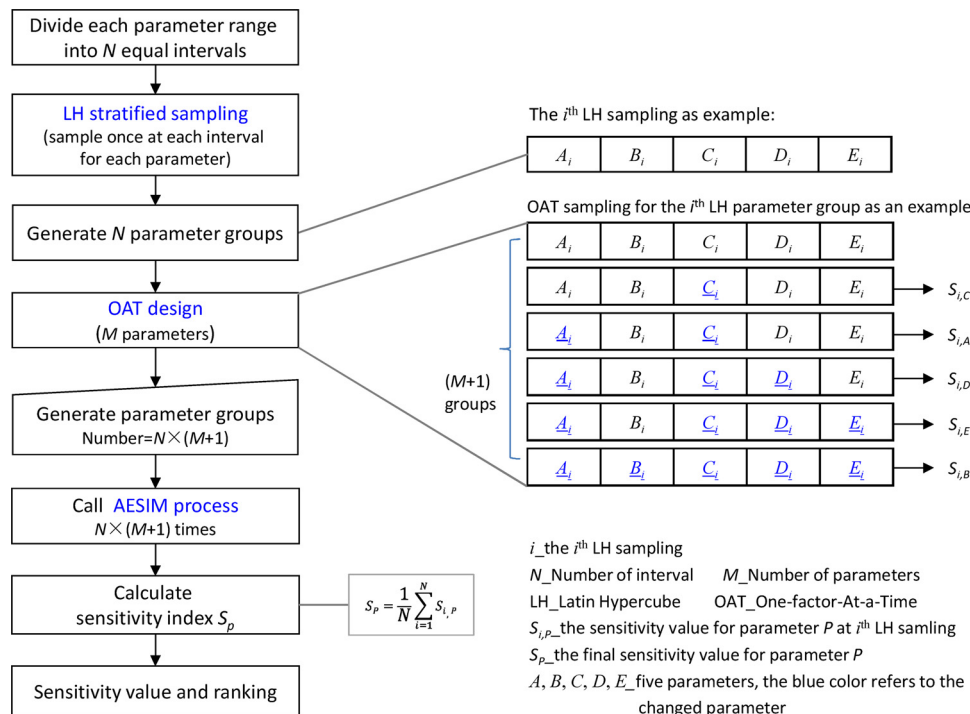


Fig. 2. The flow chart of the GSA (Global-Sensitivity-Analysis) Process based on LH-OAT method.

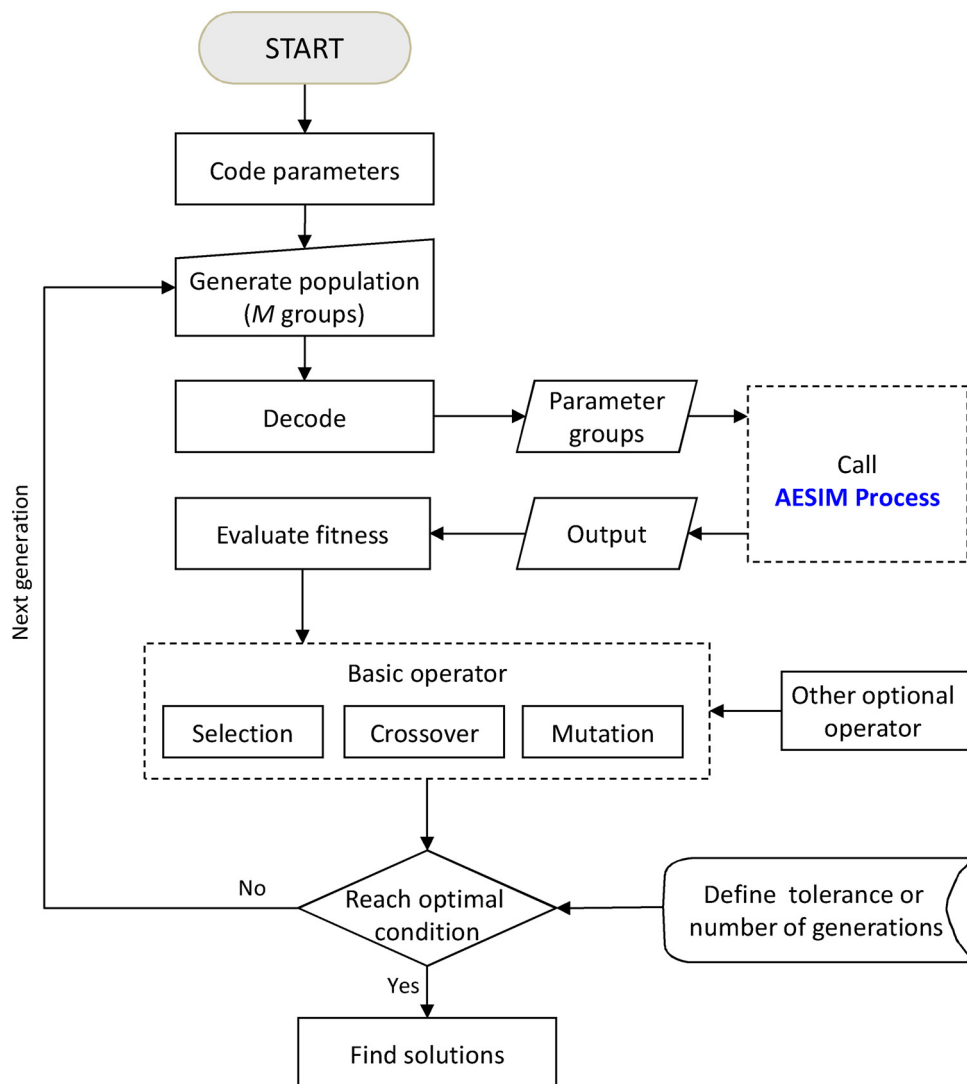


Fig. 3. The flow chart of the GPE (Global-Parameter-Estimation) Process based on modified-MGA approach.

and mutation. It represents a solution using strings (referred to as chromosomes) of variables (represented as genes) in a search problem. The search will start by initializing a population of chromosomes. Each chromosome is evaluated on its performance using a fitness function. On the basis of the performance, the chromosomes are selected into the mating pool to form offspring through the crossover and mutation of genes. Selection, crossover, and mutation are repeated for many generations to reproduce the chromosome that fits the environment best. The best chromosome would represent the optimal or near-optimal solution to the search problem (Carroll, 1998; Goldberg, 2002). The modified-MGA has been adopted to calibrate the model parameters by minimizing the error between simulated and observed data in the GPE Process.

The modified-MGA code (Carroll, 1998; Ines and Droogers, 2002) is adapted and embedded into the AHC. The parameters set with four groups are same as those in the GSA Process. The parameters selected by the GSA Process could be automatically calibrated in the GPE Process. The number of parameters is recommended not to be more than 15 to avoid the problem of non-uniqueness. The parameters related to plant growth and stress factors could generally be determined from previous literature and specific experiments. Additionally, the parameters related to solute transformation are generally difficult to be estimated inversely, and thus, they were suggested to be determined or manually calibrated on the basis of previous experimental or modeling

studies, while the parameters related to soils (mainly soil water flow and solute transport) are difficult to determine at each point of interest and are responsible for a large part of the spatial variability of the output variables. Thus, we recommend that users concern these soil parameters in the GPE Process. Similar to the sensitivity analysis, the model outputs can be optionally selected as objective variables according to the observation data collected. On the basis of these objective variables, the fitness function is constructed using the weighted average method. A more detailed description about the calculation procedures and parameter setting of the GSA Process can be found in Xu et al. (2016).

2.2.4. Graphical user interface

The GUI for the AHC is developed using the VB.NET, which is an object-oriented programming language, using the Microsoft .NET Framework 4.5 in the Visual Studio 2010 environment. The GUI allows the user to easily manipulate input files, run the model and view the output. A main window is designed as a guide for operating the AHC, including launching the windows for data input (i.e., for control file, model files, sensitivity analysis and calibration), result display, model run and exit (Fig. 4a). The control file is used for managing the file path, data file connection, function selection, simulation period, output settings, etc. In this input window, the simulation can also be customized to invoke only those modules of interest for a specified application (e.g.,

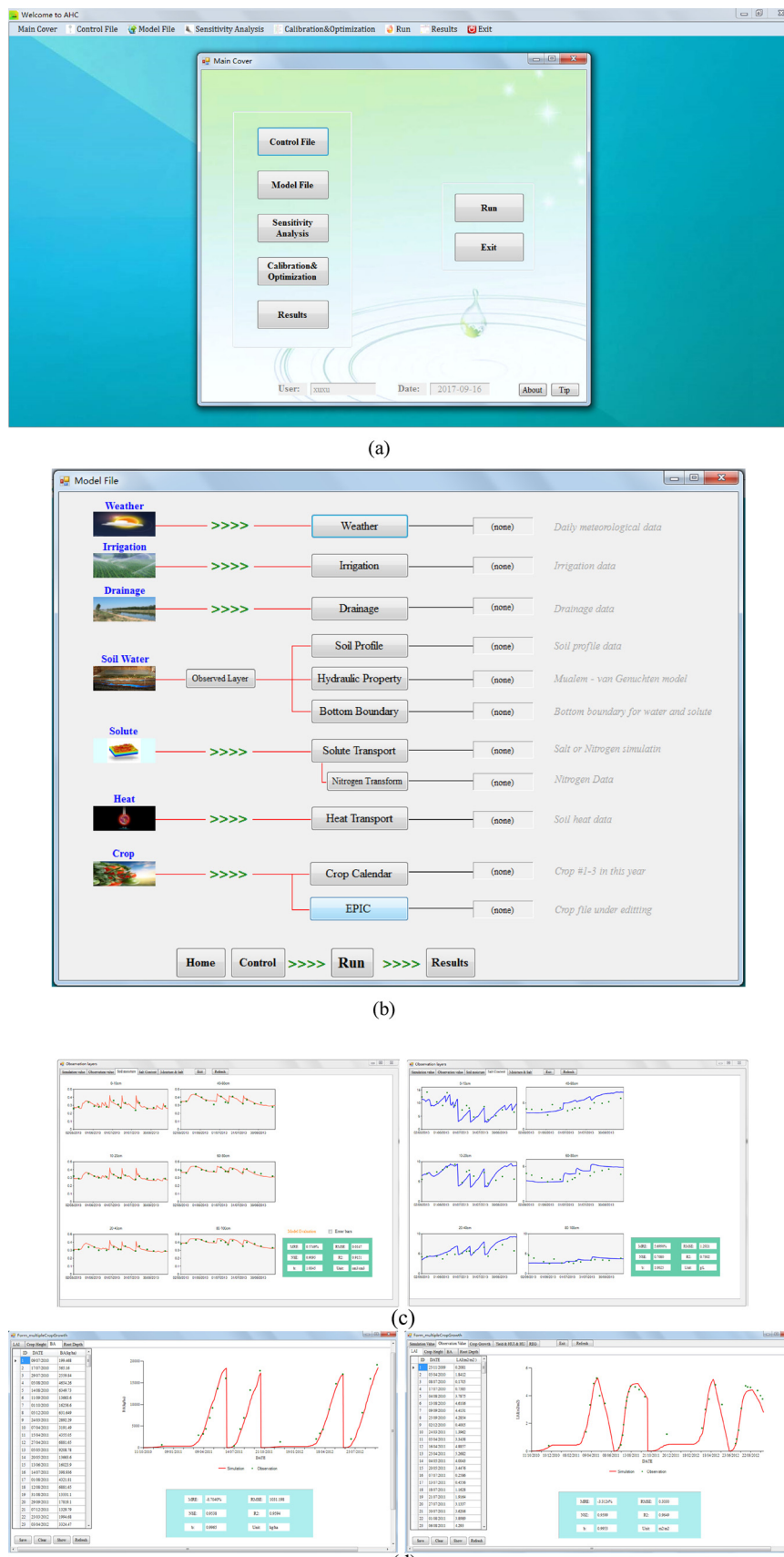


Fig. 4. Graphical user interface for the AHC – representative windows for model input and output: (a) the window for control file; (b) the window for the AESIM Process; (c) and (d) are part of the display windows for the soil water and solute output and the crop modeling output, respectively.

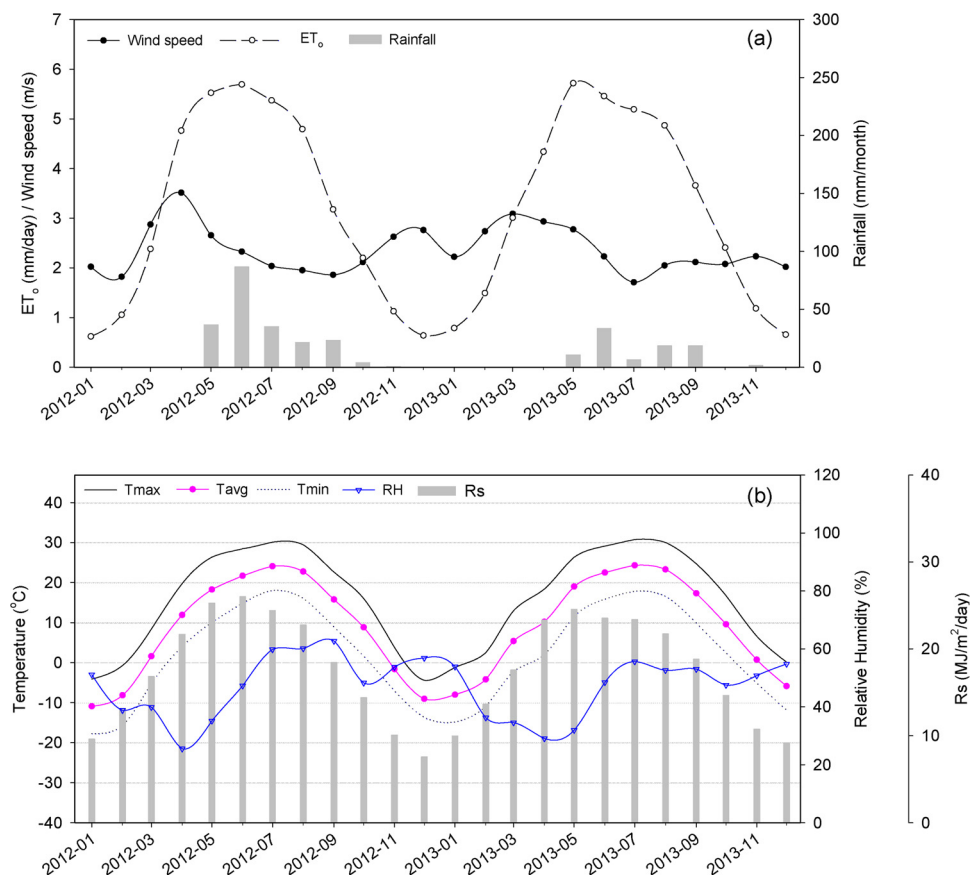


Fig. 5. Average daily wind speed and reference evapotranspiration (ET_0) and cumulative rainfall in each month (a); Average daily minimum, average and maximum temperatures (T_{\min} , T_{avg} and T_{\max}), relative humidity (RH) and solar radiation (R_s) (b) in each month at experiment site in Hetao during 2012 and 2013.

solute or heat simulation can be disabled if not desired), which can produce more efficient input operation. All data input related to the AESIM Process is integrated and shown in the input window of the model files (Fig. 4b). It could make the data input more intuitive and clearer. The input window for the sensitivity analysis and calibration is designed specifically for the data input of GSA and GPE processes, respectively. In the result display, various simulation results (e.g., soil water content, soil solution concentration/content, leaf area index and biomass) can be presented and conveniently compared with the observation data in graphics windows (Fig. 4c and d), which can help the user calibrate the model. Meanwhile, the statistical indicators (i.e., MRE, RMSE, NSE, R^2 and b) for model performance evaluation are also calculated and provided for users.

The efficiency and stability of the GUI is also repeatedly tested with several different cases. In addition, with a slight adaptation, the AHC model has been closely linked to GIS software (i.e., ArcInfo 9) for regional applications in a distributed manner. A basic graphical user interface has been constructed using the Visual Basic language (Xu et al., 2011; Jiang et al., 2015); however, it is undergoing an upgrade to ArcInfo 10, but not yet completely finished.

3. Model application

In this paper, the AHC model was to be evaluated and tested with two experimental datasets (i.e., related to salinity and nitrogen issues, respectively) by comparing the simulated results with the observed data. The test cases could provide a comprehensive presentation of the latest release of the AHC, especially the new functions (e.g., crop dormancy setting, compensated root water uptake, soil surface mulching, nitrogen transport and transformation, etc.). In salinity case, two-year field data during 2012 and 2013 was collected from the maize field

with plastic mulching, located at the Yangchang canal command area (YCA) of the Hetao Irrigation District (Hetao), Inner Mongolia Autonomous Region, northwest China ($40^{\circ}48'40''N$, $107^{\circ}05'15''E$, 1039 m altitude). The field condition was a representative of that in the upper Yellow River basin, i.e., affected by salinity under shallow water tables and under plastic film mulching. In particular, the good quality of observation data was helpful in evaluating the function of the automatic inverse calibration. The data was available from our previous study of Ren et al. (2016).

In the nitrogen case, the experimental data was obtained from the fields with a winter wheat-summer maize rotation system from October 2010 to September 2012 in the Shandong Agricultural University Agricultural Experiment Station (SAU-AES), Tai'an City, Shandong Province, northern China ($36^{\circ}09'37''N$, $117^{\circ}09'18''E$, 130 m altitude). The experimental site was also situated in an important food production base – NCP, where the nitrogen fertilizer is often overused by farmers to obtain high yields. The related data was available from the previous study of Liu (2014).

The model was to be automatically calibrated for both the above two cases with GSA and GPE processes. The parameters related to soil water flow and solute transport were usually most uncertain in practice. Thus only they were considered in the sensitivity analysis and automatic calibration as exemplifications in this study, also for restricting the number of calibrated parameters. Other parameter values were mainly referred to the previous literature and could be adjusted manually. The mean relative error (MRE), root mean square error (RMSE), Nash and Sutcliffe model efficiency (NSE), coefficient of determination (R^2) and coefficient of regression (b) were used to evaluate the model performance for both calibration and validation. Their definitions can be found in the previous study of Xu et al. (2013).

3.1. Case study of the salinity simulation

3.1.1. Site characteristics and observation data

The Hetao has a typically arid and semiarid continental climate. The average annual rainfall and pan evaporation (20 cm pan) were, respectively, 160 mm and 2240 mm during 1981–2009, with over 70% of the rainfall occurring between June and September. The daily meteorological data for the experimental years (2012 and 2013) were taken from the nearby Linhe weather station. Rainfall was registered by a tipping-bucket rain gauge in the field. The detailed data on the main weather variables are shown in Fig. 5. The total rainfall was 208 mm and 89 mm during the maize growth seasons in 2012 and 2013, respectively. The two years can represent a wet year and a dry year according to the hydrological frequency analysis. The groundwater depth (GWD) was very shallow and varied in the range 0.5–2.5 m during the crop season.

The soil physical properties were surveyed for the soil profile with a 300-cm depth and four horizons by Ren et al. (2016). Silt loam was the main soil texture in the YCA, with finer soils distributed below the zone root. The water content at saturation, field capacity and wilting point, dry bulk density and K_s were also measured. The main soil properties are presented in Table 1. The spring maize was sown in early May and harvested in late September, with a planting density of 62,000 plants ha^{-1} . Irrigation water diverted from the Yellow River has a salinity concentration of 0.5 g L^{-1} . Basin irrigation was applied by adopting zero-slope basin, which was the common practice in Hetao. The irrigation schedule is presented in Table 2. The other cultivation practices, including fertilizer application and pest, crop disease, and weed control were recommended by local farmer advisers.

Soil, groundwater, and crop growth were monitored in observation field from April to September in both years. Soil sampling was performed every 7–15 days using a soil auger. Soil samples were collected for every 10 cm in the top 0–20 cm layer, and in 20 cm increments below the top layer until the a 100-cm depth. The soil water content and salt content of the soil solution (C_{sw} , g L^{-1}) (i.e., soil salinity concentration) were measured for each layer. The daily GWD was recorded by a water level logger. The groundwater salinity concentration was obtained every 10 days. LAI was directly measured every 15 days, and crop yield was recorded after harvest. The detailed measurement methods were described in Ren et al. (2016).

3.1.2. Model setup for salinity case

A soil profile with a 300-cm depth was specified with four horizons according to the soil survey (Table 1). The domain was further discretized into 300 compartments with a uniform thickness of 1 cm. The simulation period was from the early May to late September, covering the maize growth period. The maximum root depth was set at 90 cm

Table 2

Crop cultivation, irrigation scheduling and fertilization in experimental sites for the salinity case (Hetao) and nitrogen case (Tai'an).

Site	Year	Crop	Growth period (d/m)	Irrigation		N fertilizer	
				Date (d/m)	Depth (cm)	Date (d/m)	Amount (kg N ha^{-1})
Hetao	2012	Spring maize	1/5 -	22/6	117	–	–
			23/9	2/8	114	–	–
		Spring maize	28/8	75	–	–	–
	2013		2/5 -	27/6	112	–	–
	Spring maize	21/9	17/7	94	–	–	
		8/8	8/8	108	–	–	
Tai'an	2010–2011	Winter wheat	11/10 -	20/	75	10/	86 ^a
			15/6	10	–	10	126
			29/3	75	–	29/3	–
		Summer maize	11/5	75	–	–	–
			22/6 -	21/6	75	19/7	210
	2011–2012	Winter wheat	30/9	–	–	–	–
			11/10 -	28/3	75	10/	86 ^a
		Summer maize	11/6	–	–	10	–
			11/5	75	–	28/3	126
			18/6 -	19/6	75	22/7	210
			29/9	–	–	–	–

Note: ^a means that the nitrogen is from diammonium phosphate applied as the basal fertilizer in pre-planting, while urea is applied by surface-broadcast in other N applications. The salt concentration of irrigation water in the salinity case changes very little and averages 0.5 g L^{-1} .

according to field observations and values found in the literature (Xu et al., 2015).

For soil water flow, the upper boundary condition was determined by the actual evaporation and transpiration rates, and the irrigation and precipitation fluxes. A time-variable pressure head was selected as the bottom boundary condition, which was defined using the observed GWDs. For solute transport, the upper and lower boundary conditions were defined by a concentration flux considering the observed salinity concentration of irrigation water and groundwater, respectively. The initial conditions of the soil water content and salinity concentration were set based on field measurements.

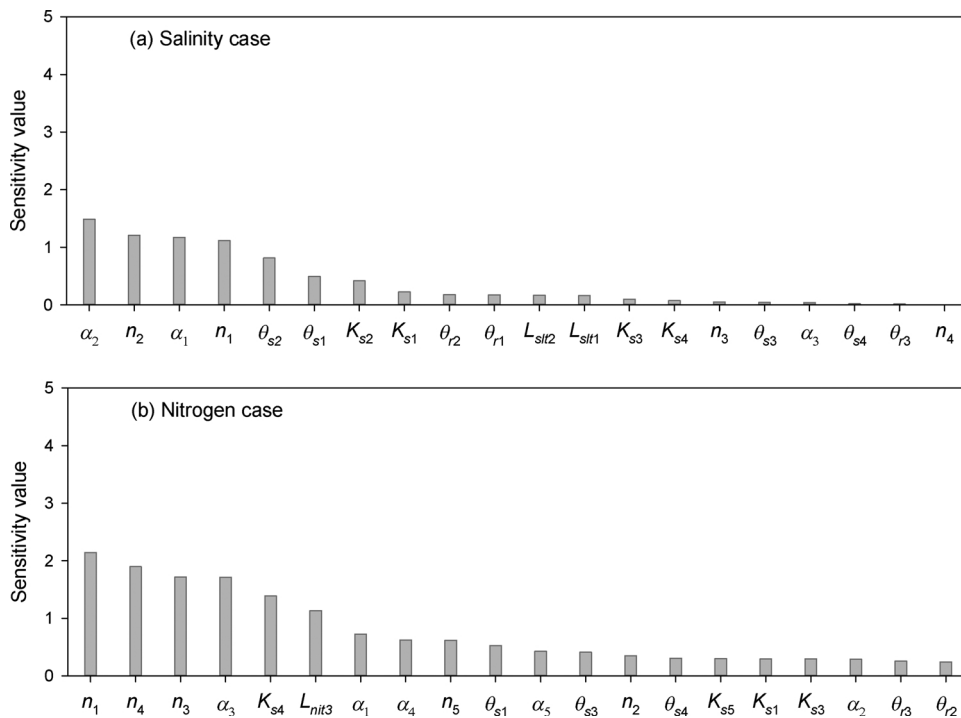
The parameters related to soil hydraulic properties, solute transport, root water uptake stress, and crop growth were initially specified before calibration. The initial values for unknown soil hydraulic parameters were estimated from the physical properties using Rosetta model (Schaap et al., 2001). Initial values for other parameters were primarily determined according to former studies (Xu et al., 2015; Ren et al., 2016; Kroes and van Dam, 2003). The measured soil water contents, salinity concentrations and LAI (as mentioned above) were used to calibrate parameters automatically using the GPE Process. Then, the

Table 1

Soil physical properties and soil hydraulic and transport parameters (calibrated values) in two experimental areas.

Site	Soil depth (cm)	Soil texture	Soil particle-size distribution (%)			Bulk density (g cm^{-3})	OMC (g kg^{-1})	Soil hydraulic parameter					
			Sand (2.0–0.05 mm)	Silt (0.05–0.002 mm)	Clay (< 0.002 mm)			θ_r ($\text{cm}^3 \text{cm}^{-3}$)	θ_s ($\text{cm}^3 \text{cm}^{-3}$)	α (cm^{-1})	n (-)	K_s (cm d^{-1})	
Hetao	0–40	Silt loam	30.4	57.5	12.1	1.43	–	0.024*	0.39*	0.013*	1.24*	27.9*	0.5 20
	40–130	Silt loam	29.5	59.6	10.9	1.38	–	0.033*	0.45*	0.009*	1.53*	18.9*	0.5 10.4*
	130–240	Silt loam	3.8	75.2	21.0	1.52	–	0.070	0.47	0.008	1.60	2.4	0.5 20
	240–300	Silt loam	34.0	58.3	7.7	1.39	–	0.040	0.45	0.010	1.61	29.6	0.5 20
	0–30	Silt loam	30.2	57.6	12.2	1.43	13.3	0.080	0.45*	0.012*	1.53*	17.0	0.5 20
	30–45	Silt loam	17.1	73.4	9.5	1.55	7.9	0.050	0.41	0.005*	1.53*	19.5	0.5 20
Tai'an	45–100	Silt	6.3	83.0	10.7	1.55	4.2	0.060	0.38*	0.007*	1.46*	15.2	0.5 16.7*
	100–160	Silt	12.8	82.8	4.4	1.52	4.1	0.050	0.41*	0.014*	1.37*	31.2*	0.5 20
	160–300	–	–	–	–	–	–	0.080	0.50	0.012	1.18*	6.3*	0.5 20

Note: the superscript * means that the corresponding parameters are highly sensitive according to GSA results, which are thus selected and calibrated in an automatic GPE Process. L refers to the dispersion length for the salt solution and $\text{NO}_3\text{-N}$ in salinity (Hetao) and nitrogen (Tai'an) cases, respectively. OMC is the soil organic matter content.



applicability of the AHC model was tested and evaluated with proper calibration and validation.

3.1.3. Results and discussion

(1) Model performance evaluation in the salinity case

The GSA results showed that only 11 of a total of 25 soil parameters were very sensitive to the observation data, with their global sensitivity values shown in Fig. 6a. Their values were inversely calibrated and are listed in Table 1. Comparisons between the simulation and observations are presented in Figs. 7–9 and Table 3. The simulated soil water contents showed good agreement with the measured soil water contents for different soil layers during 2013 (Fig. 7), resulting in a MRE = −0.86%, a RMSE = 0.015 cm³ cm⁻³, and a NSE = 0.91 (Table 3). Fig. 8 shows

that the simulated salinity concentration also fitted well with the observed one during calibration. It produced a MRE = −7.9%, a RMSE = 1.37 g L⁻¹, and a NSE = 0.67. The simulated soil water and salt dynamics by AHC were quite close to that by HYDRUS-dualKc in Ren et al. (2016). In addition, the simulated LAI and yield were in agreement with observations as well (Fig. 9a). Fitness results produced a MRE = −11.9%, a RMSE = 0.50, and a NSE = 0.87 for LAI, while the simulated crop yield (12,114 kg ha⁻¹) was only 5% lower than the observed one. Thus, the AHC performed reasonably well when simulating the soil water, salinity and crop growth during the 2013 calibration period.

The AHC model with calibrated parameters was further tested and validated with the 2012 experimental data. Soil moisture reproduced

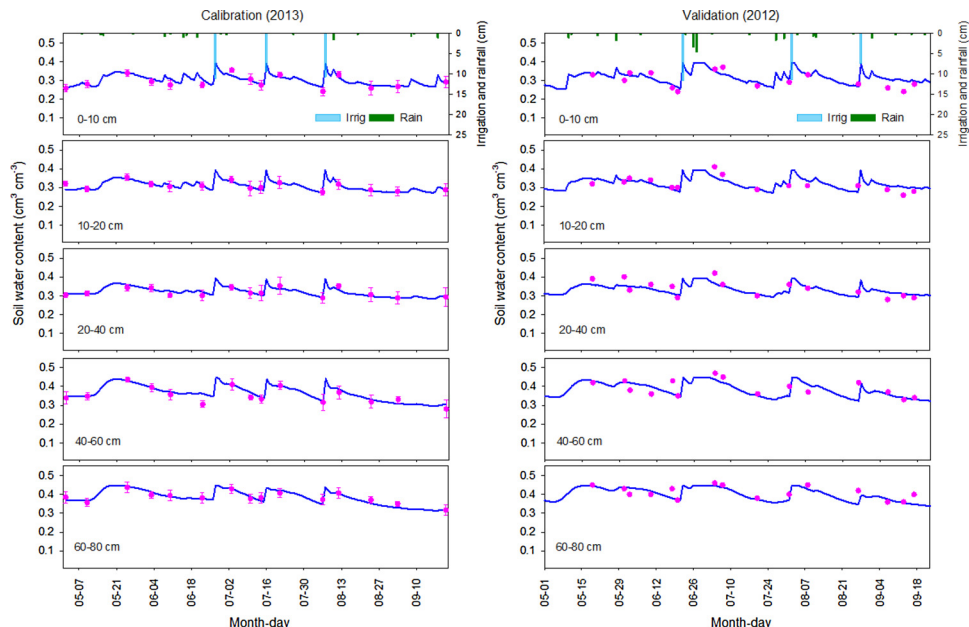


Fig. 7. Simulated versus measured soil water contents in different soil layers during model calibration (left) and validation (right) for the salinity case.

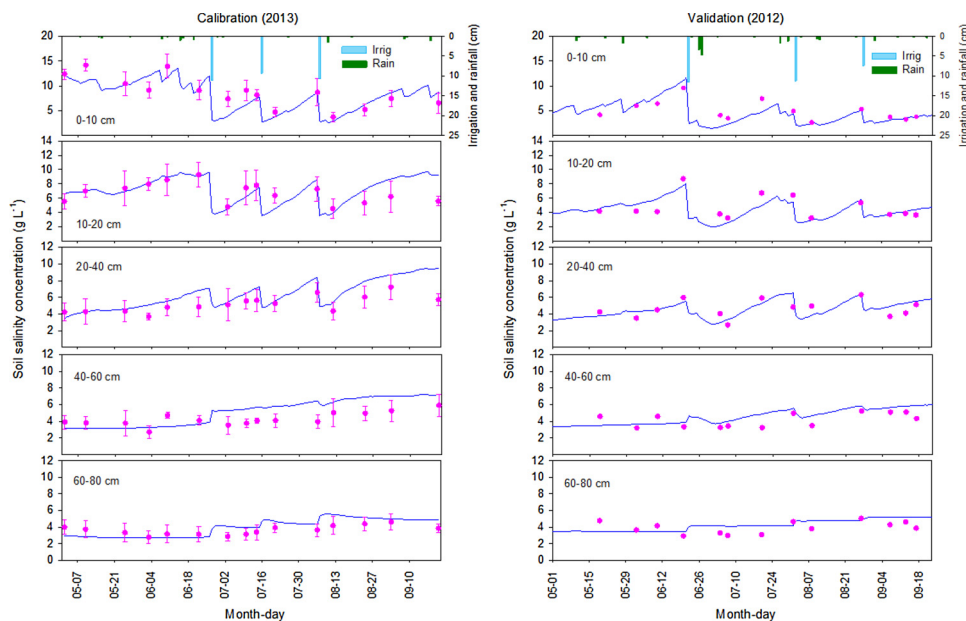


Fig. 8. Simulated versus measured soil salinity concentrations in different soil layers during model calibration (left) and validation (right) for the salinity case.

by AHC also represented the observations very well, as shown in the small errors of the estimates (Fig. 7) ($\text{RMSE} = 0.031 \text{ cm}^3 \text{ cm}^{-3}$, $\text{NSE} = 0.74$ and $R^2 = 0.75$). The simulated salinity concentration was in good agreement with observations (Fig. 8) ($\text{RMSE} = 0.99 \text{ g L}^{-1}$, $\text{NSE} = 0.42$ and $R^2 = 0.54$). The simulation for LAI seemed to be acceptable, since there were only limited observation data (Fig. 9b). The simulated yield was $12,314 \text{ kg ha}^{-1}$, 12% less than the obtained yield in 2012. Overall, the modeling accuracy of the AHC should be acceptable during the validation period. Moreover, the goodness-of-fit indicators obtained with the AHC in calibration and validation were within the range of values reported in the previous literature for field modeling cases (e.g., Jiang et al., 2011; Ramos et al., 2017; Kumar et al., 2015) and were even located at a relatively good level.

The general agreement between the simulated and measured data during calibration and validation indicated that the calibrated AHC could accurately simulate the complicated agroecosystem processes at the experimental site. Thus, it could provide useful and detailed information about the soil water and salt dynamics and maize growth, support a better understanding and solve existing problems.

(2) Simulation analysis: soil water, salinity and crop growth

The soil water and salt balance components for the 0–90 cm soil profile (i.e., the root zone) during the total simulation period of 2012 and 2013 are presented in Table 4. Simulation results indicated that the soil moisture was relatively high, fluctuating around $0.3 \text{ cm}^{-3} \text{ cm}^{-3}$ at

the surface layer and approaching saturation in deep layers both during 2012 and 2013, due to the shallow GWD and large irrigation. It increased rapidly with irrigation and then gradually decreased due to water consumption and redistribution until the next irrigation or significant rainfall event occurred (Fig. 7). In the meantime, the salinity concentration decreased sharply after an irrigation event because the soil solution was diluted and salts were leached to the deeper layers (Fig. 8). The up and down movement of soil water and salt was also partly affected by regional groundwater table fluctuations, especially for deeper soil layers. The effective rainfall was usually small in Hetao and its effects on soil moisture and salinity were mainly limited to the surface soil layer (i.e., 0–20 cm).

The results showed that maize growth was primarily stressed by salinity and temperature but not water deficit. During the early growth period, the temperature was relatively low in 2012 (Fig. 5), which was the main limiting factor for maize growth. In contrast, the salinity was higher in upper layers (e.g., $6–8 \text{ g L}^{-1}$ for solution at 10–40 cm) during the early period in 2013 (Fig. 8), and thus became the dominant stress to seedling growth (Fig. F1). Overall, a few differences were observed for crop growth in the initial stage between 2012 and 2013. However, during 2012, the crop growth was significantly affected by waterlogging due to a large rainfall event (80 mm) immediately after the first irrigation in late June (Figs. 7 and F1) that resulted in the retardation of crop growth in the vegetative period. Since late June, when there was

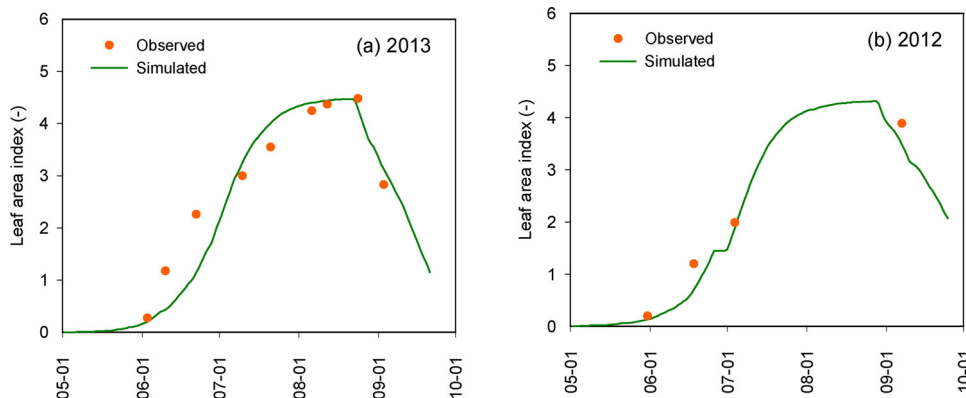


Fig. 9. Simulated versus measured leaf area index (LAI) in different soil layers during model calibration (left) and validation (right) for the salinity case.

Table 3

Goodness-of-fit test indicators relative to model calibration and validation for the salinity and nitrogen cases.

Salinity case in Hetao						
	Items	MRE (%)	RMSE	NSE	R ²	b
Calibration (2013)	Soil water content (cm ³ cm ⁻³)	−0.86	0.015	0.91	0.91	1.01
	Salinity concentration (g L ⁻¹)	−7.9	1.37	0.67	0.72	1.03
	LAI (cm ² cm ⁻²)	−11.9	0.50	0.87	0.93	1.00
Validation (2012)	Soil water content (cm ³ cm ⁻³)	1.03	0.031	0.74	0.75	1.02
	Salinity concentration (g L ⁻¹)	−4.71	0.99	0.42	0.54	1.01
	LAI (cm ² cm ⁻²)	−23.1	0.33	0.94	0.98	0.88
Nitrogen case in Tai'an						
	Items	MRE (%)	RMSE	NSE	R ²	b
Calibration (2010-2011)	Soil water content (cm ³ cm ⁻³)	3.63	0.039	0.77	0.80	0.96
	NO ₃ -N content (mg kg ⁻¹)	−21.9	6.47	0.33	0.39	0.95
	LAI (cm ² cm ⁻²)	4.0	0.21	0.98	0.99	1.02
Validation (2011-2012)	Aboveground biomass (kg ha ⁻¹)	−2.6	1214	0.95	0.96	1.00
	Soil water content (cm ³ cm ⁻³)	0.66	0.028	0.85	0.88	1.00
	NO ₃ -N content (mg kg ⁻¹)	−58.9	7.95	0.10	0.25	0.92
	LAI (cm ² cm ⁻²)	−10.8	0.40	0.92	0.95	0.94
	Aboveground biomass (kg ha ⁻¹)	−23.9	1296	0.97	0.99	0.94

MRE, mean relative error; RMSE, root mean square error; NSE, Nash and Sutcliffe model efficiency; R², coefficient of determination; b, regression coefficient; LAI, leaf area index.

Table 4

Water and salt balance in the 0–90 cm soil profile (i.e., the root zone) during the maize growing seasons in 2012 and 2013 for the salinity case in Hetao.

Items	2012		2013	
	Water (mm)	Salt (mg cm ⁻²)	Water (mm)	Salt (mg cm ⁻²)
Season irrigation	306	15.3	314	15.7
Season rainfall	202	0	88	0
Interception	12	0	8	0
Capillary rise	281	96.2	337	93.4
Percolation	164	67.2	103	39.9
Actual transpiration, T_a	443	0	488	0
Actual evaporation, E_a	188	0	171	0
Initial storage	302	106.7	302	126.3
Final storage	284	151.2	271	195.5

almost no temperature stress, the water uptake and growth of maize were mainly affected by salinity levels (Fig. F1). It was obvious that the salinity concentration and salt stress was markedly higher in 2013 than in 2012 (Figs. 8 and F1). Because the higher rainfall in 2012 (202 mm) can lead to the greater salt leaching and 100 mm less capillary rise, there is less salt accumulation into the root zone (Table 4). Thus, the maize could then grow better in 2012. In particular, the salinity concentration was relatively high during the key period of the reproductive period (i.e., after mid-August) in 2013. Overall, the crop yield was relatively higher in 2012 than in 2013. In both 2012 and 2013, it was found that most of the leached salts could not be discharged timely and stayed in the deeper soil layers due to a poor drainage system. These salts would reaccumulate into the upper layers with the upward water movement under the arid climate in Hetao. In summary, this test case

testing showed that the AHC can well reflect the soil water-salt dynamics and interaction with maize growth. Additionally, it indicated that the key issue was the reasonable control of shallow water tables and coordination of irrigation and drainage in Hetao.

3.2. Case study of the nitrogen simulation

3.2.1. Site characteristics and observation data

The SAU-AES is located in the southern NCP. This region has a temperate continental monsoon climate. The mean annual rainfall is 697 mm, 70–80% of which occurs between June and September. Daily meteorological data for 2007 and 2008 were available from the nearby Tai'an weather station. The detailed data on the main weather variables are shown in Fig. 10 for both experimental years. The depth of the groundwater is greater than 10 m during the year.

Silt loam and silt are the main soil textures for topsoil and subsoil, respectively, with four horizons in the 0–160 cm soil profile in SAU-AES. The principle soil characteristics are listed in Table 1. The water contents at saturation, field capacity and wilting points, the K_s and the organic matter content (OMC) were measured for each horizon. In addition, the soil fertility properties of the upper soils (0–45 cm) were as follows: soil organic matter, 7.9–13.3 g kg⁻¹; total N, 0.66–1.12 g kg⁻¹; available phosphorous, 34.1–66.1 mg kg⁻¹; and available potassium, 74.9–121.7 mg kg⁻¹. The related measurement approaches were described in detail by Liu (2014).

The cropping system was the rotation of winter wheat and summer maize that was common in NCP. The planting density was 2.4 M plants ha⁻¹ and 66,000 plants ha⁻¹, respectively. The irrigation and fertilization schedules were determined as recommended by local farmer advisers (Table 2). Irrigation water was pumped from groundwater. The food irrigation was adopted and the surface-broadcast of urea was applied as the topdressing of fertilizer N, which were both the common practices in the NCP. Other cultivation practices related to pest, crop disease, and weed control were recommended by farmer advisers.

Soil and crop growth were monitored during the two agricultural years from 2010 and 2012. The soil water content was measured at 20 cm increments from soil surface down to a 160-cm depth using a neutron probe, with a frequency of 10 days. The nitrate-nitrogen (NO₃-N) contents were measured approximately every 30 days for the same layers. LAI and D-AGB were measured every month. The dry grain yield was weighed after harvesting. The detailed measurement methods can be found in Liu (2014).

3.2.2. Model setup for nitrogen case

A soil profile with a 300-cm depth was specified to have five material horizons. For depths below 160 cm, the soil properties were initially assumed to be the same as the last observed layer. In vertical discretization, the soil domain was discretized into 200 compartments with uniform 1-cm thickness for the first 100 cm depth and 2-cm thickness for 100–300 cm. The simulation period was from October 3rd, 2010 to September 30th, 2012, covering two seasons of the rotation of wheat and maize.

For soil water flow, the upper boundary condition was determined by the actual evaporation and transpiration rates and the irrigation (Table 2) and precipitation fluxes. The surface mulch by wheat straw was considered to estimate E_a during the maize season. At the bottom, a free drainage boundary condition was used to account for the deep GWD. For nitrogen transport, the upper and lower boundary conditions were defined as the third-type boundary conditions by specifying a concentration flux using the concentration of NO₃-N and ammonia-nitrogen (NH₄-N) in irrigation water, rainfall and groundwater. For heat transport, the daily average air temperature was used to define top boundary condition. If there was rainfall or irrigation, third-type boundary condition was used to prescribe the top heat flux. The third-type boundary condition was also applied at the bottom to specify the heat flux. The initial conditions of soil water content, nitrogen

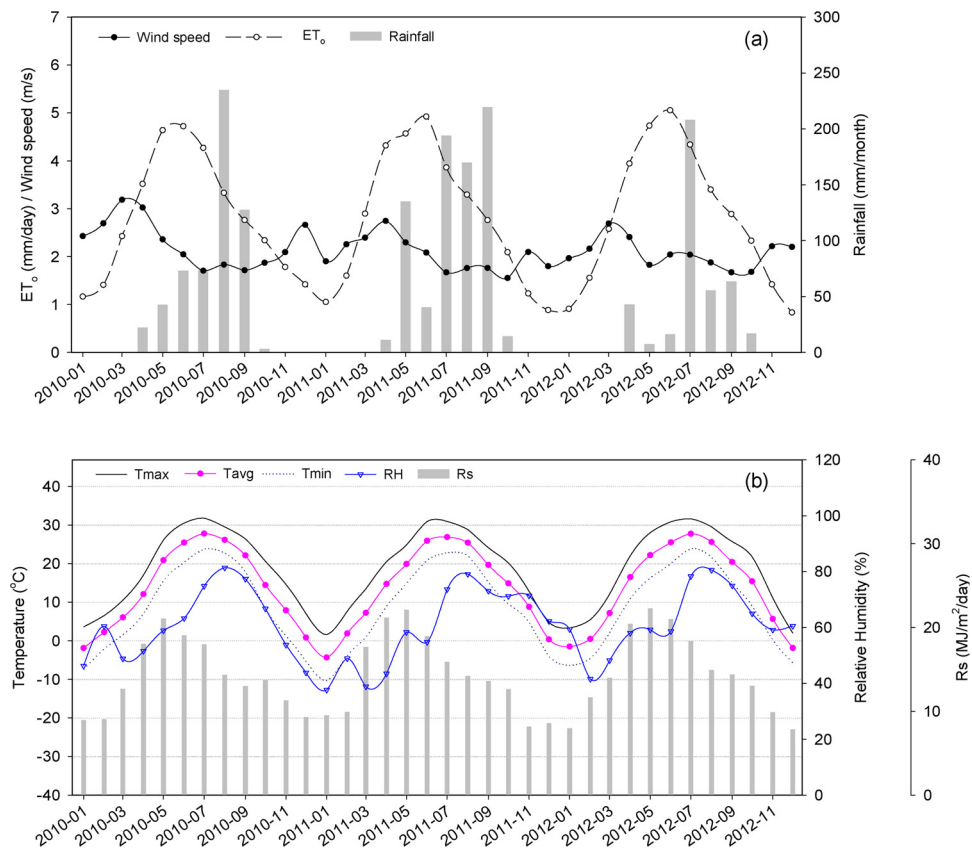


Fig. 10. Average daily wind speed and reference evapotranspiration (ET_0) and cumulative rainfall in each month (a); Average daily minimum, average and maximum temperatures (T_{\min} , T_{avg} and T_{\max}), relative humidity (RH) and solar radiation (R_s) (b) in each month at the experiment site in Tai'an during 2010–2012.

concentration and temperature were set based on field observations. The crop dormancy was considered for wheat growth in the winter season.

The parameters related to soil hydraulic properties, nitrogen transport and transformation, root water uptake stress and crop growth were initially specified before calibration. The unknown soil hydraulic parameters (Table 1) were initialized with the physical properties using the pedotransfer functions (PFTs) of Wösten et al. (1999). The parameters related to carbon turnover were assigned according to Hansen et al. (1991). The values of other parameters were initialized according to previous studies (Liu, 2014; Ahuja et al., 2000; Williams et al., 2006; Wang, 2010). Initial values of crop parameters for spring wheat and summer maize were defined on the basis of our previous research in the NCP (Wang et al., 2015; Wang, 2010). The measured soil water contents, $\text{NO}_3\text{-N}$ contents, LAI and D-AGB (as mentioned above) were used for parameter estimation through the GPE Process. Modeling results were also evaluated by comparison with those using the RZWQM2 model by Liu (2014).

3.2.3. Results and discussion

(1) Model performance evaluation in the nitrogen case

The GSA showed that 15 of a total of 35 soil parameters were very sensitive to the observation data, with their global sensitivity values shown in Fig. 6b. The calibrated values for model parameters are presented in Table 1. The comparisons of simulated and measured soil water contents and $\text{NO}_3\text{-N}$ contents at different layers are presented in Figs. 11 and 12, respectively, both for the calibration (2010–2011) and validation (2011–2012). The results showed that the simulated soil water contents were in a good agreement with the measured soil water contents for various soil layers during 2010–2012 (Fig. 11). The RMSE was less than $0.04 \text{ cm}^3 \text{ cm}^{-3}$ for both calibration and validation, while the NSE reached to over 0.77 (Table 3). The fitness was even better than

that of Liu (2014), who used the RZWQM2. Additionally, because the AHC took into account the crop dormancy and effects of soil frost on hydraulic conductivity, the water could be held in the soil layer and the soil moisture changed slightly during the crop dormancy period (Fig. 11). The simulation seemed to be more reasonable during the winter season than that of the RZWQM2 of Liu (2014). Moreover, the simulated surface soil moisture became large after high rainfall and could even approach saturation, which was not captured by RZWQM2. This was because the AHC allowed surface ponding to consider the effects of soil bunds, while the storage of surface runoff was not considered in RZWQM2. The simulated $\text{NO}_3\text{-N}$ contents were also in a reasonable agreement with the measured ones (Fig. 12). Simulation of N fate was intrinsically more difficult than that for other terms, due to the complex processes of N transport and transformation. Surface-broadcast of urea would increase the uncertainty in observations. In spite of that, the AHC reasonably captured the dynamics of the observed $\text{NO}_3\text{-N}$ contents. In particular, the $\text{NO}_3\text{-N}$ variations were relatively large in near-surface layer and were well described using the AHC. In addition, the simulated $\text{NO}_3\text{-N}$ variations by the AHC were also better than that by RZWQM2 (Liu, 2014). The goodness-of-fit indicators obtained with the AHC during the two years (Table 3) were within the range of values reported in previous studies (e.g., Cameira et al., 2007; Wang and Huang, 2008; Liu, 2014; Liang et al., 2014). For crop growth, the simulated LAI and D-AGB matched quite well with the observations (Fig. 13), with very good fitness indicator values both in calibration and validation (Table 3). Meanwhile, simulated grain yields for wheat (7776 kg ha^{-1} and 7597 kg ha^{-1}) had relative errors of less than 5% in the two seasons and that for maize (8741 kg ha^{-1} and 9762 kg ha^{-1}) had relative errors of less than 6%. Thus, the AHC performed reasonably well in simulation during the calibration and validation periods of 2010–2012.

(2) Simulation analysis: soil water, nitrogen and crop growth

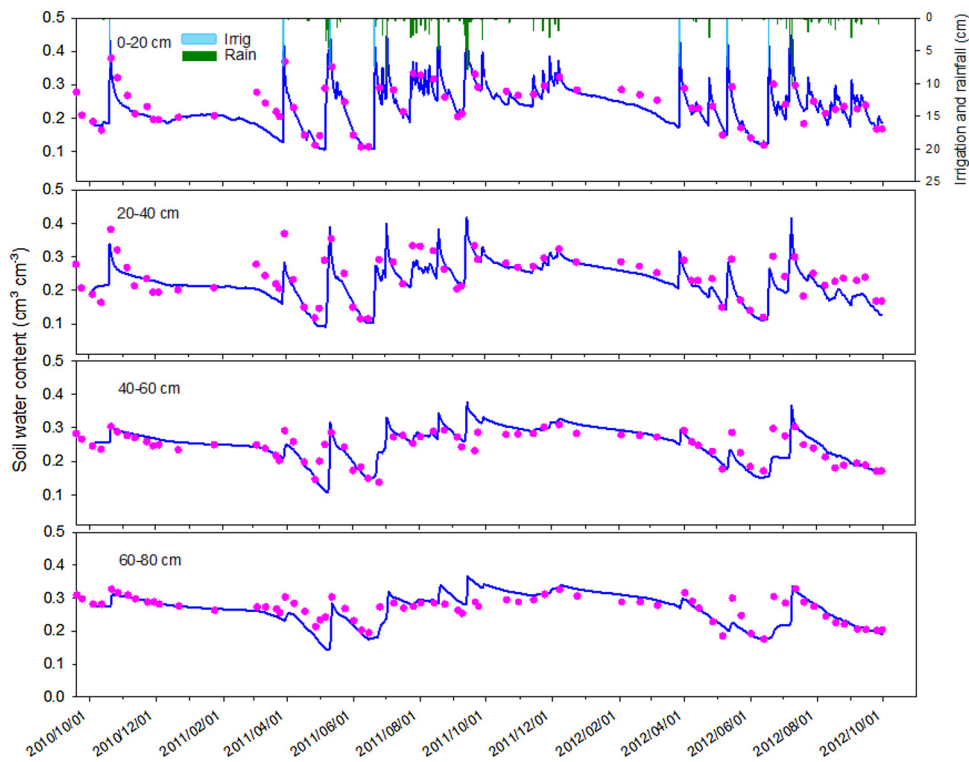


Fig. 11. Simulated versus measured soil water contents in different soil layers during model calibration (Oct-2010 to Sept-2011) and validation (Oct-2011 to Sept-2012) for the nitrogen case.

The water and nitrogen balance components for the 0–100 cm soil profile (i.e., root zone) are presented in Table 5. The results showed that irrigation and rainfall were mainly consumed by ET during the wheat season. The ET_a was 504 and 514 mm for spring wheat in the first and second seasons, respectively, while T_a was 47 mm greater for the first

season (2010–2011) because of larger LAI in vegetative growth stage. The bottom flux of the root zone (i.e., at 100 cm in depth) was small and almost moved upward after turning green (March to early June). This was because there was often less rainfall during the spring season in NCP and the applied irrigation (75 mm) was not excessive. In

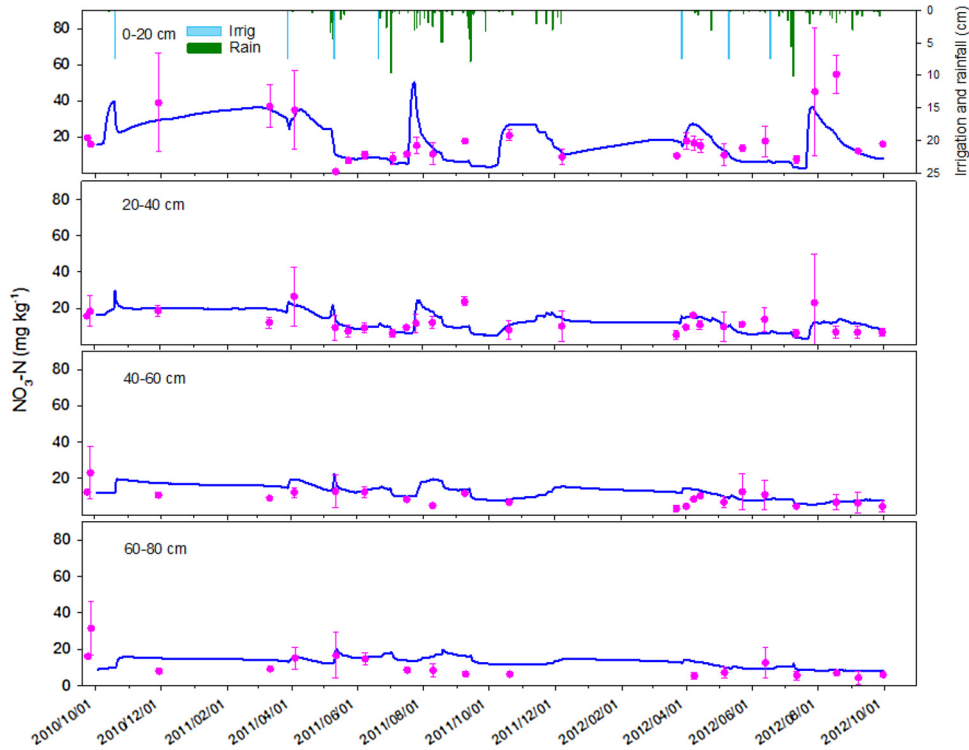


Fig. 12. Simulated versus measured $\text{NO}_3\text{-N}$ contents in different soil layers during model calibration (Oct-2010 to Sept-2011) and validation (Oct-2011 to Sept-2012) for the nitrogen case.

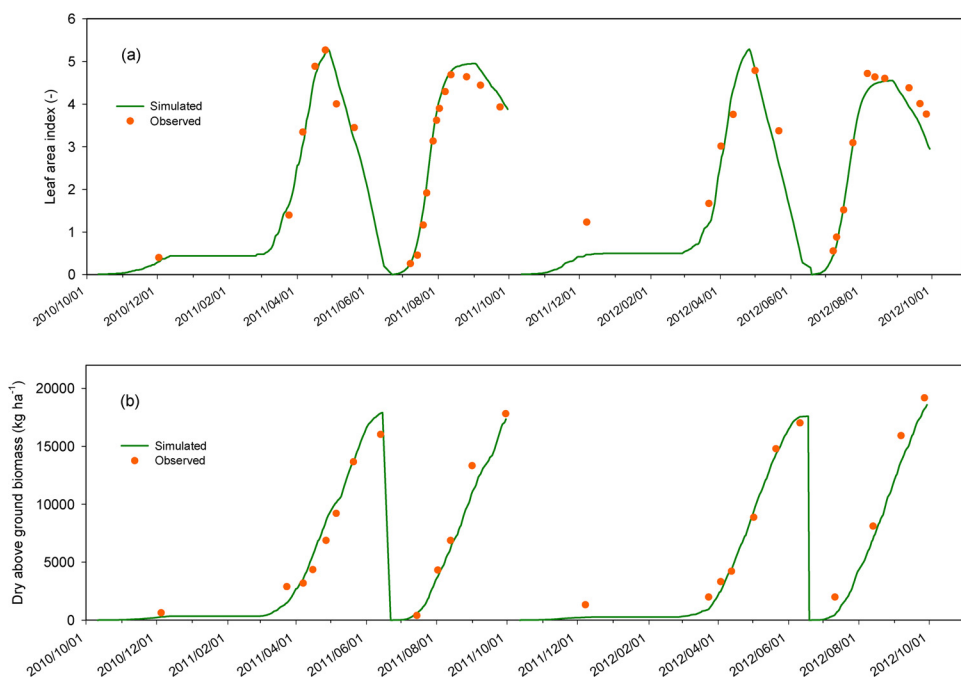


Fig. 13. Simulated versus measured data: (a) leaf area index; (b) dry aboveground biomass in the nitrogen case during calibration (Oct-2010 to Sept-2011) and validation (Oct-2011 to Sept-2012).

Table 5

Water and nitrogen balance in the 0–100 cm soil profile (i.e., the root zone) for seasons of winter wheat and summer maize during 2010–2011 and 2011–2012 in Tai'an.

Items	2010–2011		2011–2012	
	Wheat	Maize	Wheat	Maize
Irrigation	225	75	150	75
Rainfall	139	597	160	324
Wqbot	47	-120	44	-2
T _a	386	301	339	303
E _a	118	65	175	69
Storage change	-92	186	-182	26
Nfert	212.0	210.0	212.0	210.0
Nnmin	79.6	70.6	47.9	62.2
Nra_ir	18.2	33.6	15.5	20.0
Nvol	55.1	75.4	52.6	79.5
Nupt	285.1	196.7	271.1	211.3
Nnbot	29.6	-95.0	34.1	3.0
Nden	1.5	3.7	0.6	1.3
Storage change	0.1	-54.4	-11.9	5.6

Note: The units for water balance terms and nitrogen balance terms are mm and kg N ha⁻¹, respectively.

Wqbot, cumulative water flux at bottom of root zone (positive for upward); T_a, actual transpiration; E_a, actual evaporation.

Nfert, N fertilizer; Nnmi, net mineralization; Nra_ir, N in rainfall and irrigation water; Nvol, N volatilization; Nupt, crop N uptake; Nnbot, net cumulative N flux at the bottom (positive for upward); Nden, N denitrification.

particular, the wheat was not timely irrigated during the second irrigation event in the first season, which caused water stress to some degree (Fig. F2). This also happened in the second season (2011–2012) but occurred before the third irrigation event. Overall, during the two seasons, the wheat growth was affected by low temperatures during early stage of the turning green period (March) and water deficit in the following stages but was almost not affected by nitrogen deficiency (Fig. F2). Thus, with similar climate conditions (especially temperature and radiation), the wheat yield was very similar in the two seasons. The above analysis was also similar to that using the RZWQM2 (Liu, 2014).

The maize was generally irrigated no more than once, as it grew in the summer rainy season, with rainfall of 597 mm and 324 mm during the first season (2011) and second season (2012), respectively. The results showed that the *ET_a* of summer maize was approximately 370 mm for both two seasons, with slight differences for both *E_a* and *T_a*. The rainfall was obviously greater during 2011 (Figs. 10 and 11); thus, the deep percolation from the root zone was also more significant during this season (reaching to 120 mm), and the water storage was increased by 186 mm after harvest (Table 5). There was almost no surface runoff in the two seasons due to the effects of soil bunds (10 cm). Overall, the stress from water deficit was very small for maize growth because of the plentiful rainfall in the summer rainy season. Maize growth was mainly affected by nitrogen deficit in the seedling period, which was more obvious during 2012 (Fig. F2). However, the grain yield was still 11% higher in 2012 than that in 2011 due to the higher solar radiation, with a similar cumulative temperature during the maize season from June to September in 2012 (Fig. 10).

Simulated results indicated that the nitrogen was mainly consumed by crop nitrogen uptake which accounted for approximately 80% and 50–70% of total N consumption during the wheat and maize growth periods, respectively. The nitrogen was primarily lost through NH₃ volatilization after irrigation, reaching to approximately 130 kg ha⁻¹ in 2011 and 2012 and accounting for approximately 20% of total N consumption. The nitrogen leaching was only significant during the maize growth period (i.e., summer rainy season) in the wet year of 2011. The amount of 121.9 kg ha⁻¹ nitrogen was leached out of the root zone (0–100 cm), and only 22% could be reused by capillary rise. Thus, the net leaching loss reached to 95.0 kg ha⁻¹, which composed 25% of the total nitrogen loss (Table 5). For the wheat growth period (spring dry season) and maize growth period in 2012 (lower rainfall season compared to 2011), the amount of nitrogen leaching was less than 32 kg ha⁻¹ for the root zone. This was also because the irrigation amount was limited in the experiment. It was even less than the upward recharge from the underlying layers for wheat growth. Thus, this resulted in an upward cumulative flux of approximately 30 kg ha⁻¹ during the two seasons (Table 5). In addition, the results also showed that the net leaching loss at 200 cm in depth was less than 20 kg ha⁻¹ both for 2010–2011 and 2011–2012. The results indicated that the

denitrification loss just occupied a very small part and could almost be neglected. The results for the nitrogen budget by the AHC were similar to those from using RZWQM2 (Liu, 2014). Thus, the control of NH₃ volatilization should receive attention even with relatively reasonable irrigation scheduling. In summary, the test case indicated that the AHC should be a reliable tool to simulate the water and nitrogen fate and the related crop growth in the field.

4. Summary and conclusion

A new physically based numerical model (named AHC) that was developed to simulate the agroecosystem processes was presented in this paper. The model concept, algorithm and structure of the AHC were described in detail, with a brief description of the software user interface. The model was designed with three main processes (i.e., the AESIM, GSA and GPE processes) each of which consisted of many modules for implementing specific functions. The AESIM Process simulated the soil water flow, the fate of salt or nitrogen, and heat transport in a mechanical process-based manner. That is, it was all based on the numerical solution of a series of partial differential equations. Thus, the AHC model was also suitable to very complex agro-hydrological conditions. The generic crop growth module was drawn from the concept of the EPIC model, which was suitable for various plant species with acceptable accuracy and less data demand. The GSA and GPE processes were used in conjunction to determine the parameters during model calibration based on the LH-OAT and modified-MGA methods.

Relative to the other agroecosystem models, there were three significant features of the AHC: (1) the ability to optionally simulate the fate of nitrogen and the fate of salt; (2) the robust ability to do global parameter sensitivity analysis and to inversely calibrate the model parameters; and (3) the adaptability to a wide range of field conditions, especially some specific phenomena or farm practices in northern China (e.g., crop dormancy, soil frost and thaw in winter and different film mulching).

The AHC was then tested with using the data from two typical field experiments that were related to the salinity issue in a maize field in northwest China and the nitrogen use for a wheat-maize rotation field on North China Plain, respectively. Two years of data were used to evaluate the model performance in both cases. Eleven sensitive parameters and fifteen ones of all soil hydraulic and transport parameters were screened out for the model calibration in salinity and nitrogen cases, respectively. The results indicated that the model can accurately capture the dynamics of layered soil water contents. The simulated crop indicators (leaf area index, biomass and yield) were also in a quite good agreement with the observations. With regard to the solute, the AHC could predict the soil salinity concentration well. The simulation accuracy for nitrogen fate was acceptable compared to previous studies, but yet not as good as that for salt. This should be related to the complex mechanism of nitrogen fate and the high spatial variation caused by surface broadcast fertilization. In conclusion, all indicators supported the ability of the model to simulate the agroecosystem processes. Furthermore, the issues related to field irrigation water use, the salinity effect, nitrogen use efficiency, etc., were evaluated using the calibrated model.

Taken as a whole, the AHC should prove to be a reliable and efficient tool in analyzing the complex agroecosystem processes and in supporting the rational management of irrigation application, salinity control and nitrogen fertilizer use. In the subsequent development of the AHC model, the focus is to improve the description of the agroecosystem, including adding process descriptions of phenomena that are not yet included in the current version, e.g., the soil freezing and thawing, the effects of soil tillage on transport processes, and pesticide transport. Another important focus is to better support distributed modeling for regional land and water management.

Acknowledgements

This research was supported by the National Natural Science Foundation of China (grant numbers: 51639009, 51679235, 51209204 and 51125036) and the 13th Five-year National Key Research and Development Program of the Chinese Ministry of Science and Technology (grant numbers: 2016YFC0400107). We also acknowledge Professor Kelin Hu and Dr. Hao Liang from China Agricultural University for their kind help in testing the model of the nitrogen simulation.

Appendix A. Supplementary data

Supplementary material related to this article can be found, in the online version, at doi:<https://doi.org/10.1016/j.ecolmodel.2018.10.015>.

References

- Abbaspour, K.C., Schulin, R., van Genuchten, M.T., 2001. Estimating unsaturated soil hydraulic parameters using ant colony optimization. *Adv. Water Resour.* 24 (8), 827–841.
- Ahuja, L.R., Rojas, K.W., Hanson, J.D., Shaffer, M.J., Ma, L., 2000. The Root Zone Water Quality Model. Water Resources Publ., LLC, Highlands Ranch, CO, pp. 372.
- Borg, H., Grimes, D.W., 1986. Depth development of roots with time: an empirical description. *Trans. ASAE* 29 (1), 194–197.
- Cameira, M.R., Fernando, R.M., Ahuja, L.R., Ma, L., 2007. Using RZWQM to simulate the fate of nitrogen in field soil–crop environment in the Mediterranean region. *Agric. Water Manag.* 90 (1–2), 121–136.
- Carroll, D.L., 1998. GA Fortran Driver Version 1.7 [EB/OL]. <http://www.cuaerospace.com/carroll/ga.html>.
- Coucheney, E., Buis, S., Launay, M., Constantin, J., Mary, B., García De Cortázar-Atauri, I., et al., 2015. Accuracy, robustness and behavior of the STICS soil-crop model for plant, water and nitrogen outputs: evaluation over a wide range of agro-environmental conditions in France. *Environ. Model. Softw.* 64, 177–190.
- De Vries, D.A., 1975. Heat transfer in soils. In: De Vries, D.A., Afgan, N.H. (Eds.), *Heat and Mass Transfer in the Biosphere. I. Transfer Processes in Plant Environment*. Scripts Book Company, Washington DC, pp. 5–28.
- DeJonge, K.C., Ascough II, J.C., Ahmadi, M., Andales, A.A., Arabi, M., 2012. Global sensitivity and uncertainty analysis of a dynamic agroecosystem model under different irrigation treatments. *Ecol. Modell.* 231, 113–125.
- Della Peruta, R., Keller, A., Schulin, R., 2014. Sensitivity analysis, calibration and validation of EPIC for modelling soil phosphorus dynamics in Swiss agro-ecosystems. *Environ. Model. Softw.* 62, 97–111.
- Doherty, J., 2005. PEST: Model-Independent Parameter Estimation, User Manual, 5th ed. Watermark Numerical Computing, Brisbane, Australia.
- Duan, Q., Sorooshian, S., Gupta, V.K., 1994. Optimal use of the SCE-UA global optimization method for calibrating watershed models. *Journal of Hydrology* 158 (3–4), 265–284.
- Evensen, G., 2003. The Ensemble Kalman Filter: theoretical formulation and practical implementation. *Ocean Dyn.* 53 (4), 343–367.
- Goldberg, D.E., 1989. *Genetic Algorithms in Search, Optimization and Machine Learning*. Addison-Wesley, Reading, Mass.
- Goldberg, D.E., 2002. *. The Design of Innovation: Lessons From and for Competent Genetic Algorithms*, 7. Springer Science & Business Media.
- Hansen, S., 2002. Daisy, a flexible soil-plant-atmosphere system model. *Rep. Dept. Agric.*
- Hansen, S., Jensen, H.E., Nielsen, N.E., Svendsen, H., 1991. Simulation of nitrogen dynamics and biomass production in winter wheat using the Danish simulation model DAISY. *Fertil. Res.* 27 (2–3), 245–259.
- Holland, J.H., 1975. *Adaptation in Natural and Artificial Systems*. University of Michigan Press, Ann Arbor.
- Hoogenboom, G., Jones, J.W., Wilkens, P.W., Porter, C.H., Boote, K.J., Hunt, L.A., et al., 2015. Decision Support System for Agrotechnology Transfer (DSSAT) Version 4.6. DSSAT Foundation, Prosser, Washington. <http://dssat.net>.
- Ines, A.V.M., Droogers, P., 2002. Inverse modelling in estimating soil hydraulic functions: a Genetic Algorithm approach. *Hydrol. Earth Syst. Sci.* 6 (1), 49–66.
- Jarvis, N.J., 1989. A simple empirical model of root water uptake. *J. Hydrol.* 107 (1–4), 57–72.
- Jiang, J., Feng, S., Huo, Z., Zhao, Z., Jia, B., 2011. Application of the SWAP model to simulate water-salt transport under deficit irrigation with saline water. *Math. Comput. Model.* 54 (3–4), 902–911.
- Jiang, Y., Xu, X., Huang, Q., Huo, Z., Huang, G., 2015. Assessment of irrigation performance and water productivity in irrigated areas of the middle Heihe River basin using a distributed agro-hydrological model. *Agric. Water Manag.* 147, 67–81.
- Jones, C.A., 1985. C4 Grasses and Cereals. John Wiley and Sons, Inc., New York, pp. 412.
- Jones, J.W., Hoogenboom, G., Porter, C.H., Boote, K.J., Batchelor, W.D., Hunt, L.A., et al., 2003. The DSSAT cropping system model. *Eur. J. Agron.* 18 (3–4), 235–265.
- Jones, J.W., He, J., Boote, K.J., Wilkens, P., Porter, C.H., Hu, Z., 2011. Estimating DSSAT Cropping System Cultivar-specific Parameters Using Bayesian Techniques. *Advances in Agricultural Systems Modeling. American Society of Agronomy, Crop Science*

- Society of America, Soil Science Society of America, Madison, WI, pp. 365–394.
- Kroes, J.G., van Dam, J.C., 2003. Reference Manual SWAP Version 3.0.3, Alterra-report 773, Alterra. Green World Research, Wageningen.
- Kucharik, C.J., 2003. Evaluation of a process-based agro-ecosystem model (Agro-IBIS) across the U.S. Corn belt: simulations of the interannual variability in maize yield. *Earth Interact.* 7 (14), 1–33.
- Kumar, P., Sarangi, A., Singh, D.K., Parihar, S.S., Sahoo, R.N., 2015. Simulation of salt dynamics in the root zone and yield of wheat crop under irrigated saline regimes using SWAP model. *Agric. Water Manag.* 148, 72–83.
- Liang, H., Hu, K., Li, B., Liu, H., 2014. Coupled simulation of soil water-heat-carbon-nitrogen process and crop growth at soil-plant-atmosphere continuum system. *Trans. CSAE* 30 (24), 54–66 (in Chinese with English abstract).
- Liu, H.T., 2014. Soil Characteristics and Crop Water and Nitrogen Use Efficiencies of A High Productivity Region in the North China Plain. PhD Thesis. China Agricultural University, Beijing, China (in Chinese).
- McCown, R.L., Hammer, G.L., Hargreaves, J.N.G., Holzworth, D.P., Freebairn, D.M., 1996. APSIM: a novel software system for model development, model testing and simulation in agricultural systems research. *Agric. Syst.* 50 (3), 255–271.
- Monsi, M., Saeki, T., 1953. Über den Liefaktor in den Pflanzengesellschaften und sein Bedeutung für die Stoffproduktion. *Jpn. J. Bot.* 14, 22–52.
- Monteith, J.L., 1965. Evaporation and the environment. The State and Movement of Water in Living Organisms. Cambridge University Press, Swanssea, pp. 205–234.
- Monteith, J.L., 1996. The quest for balance in crop modeling. *Agron. J.* 88 (5), 695–697.
- Mualem, Y., 1976. A new model for predicting the hydraulic conductivity of unsaturated porous media. *Water Resour. Res.* 12 (3), 513–522.
- Neng, F.T., 2016. Agricultural Hydrology-ecosystem Modeling Software (AHC): Development and Testing. Master Thesis. China Agricultural University, Beijing, China.
- Oosterbaan, R.J., 2001. SALTMOD: Description of Principles, User Manual, and Examples of Application, Version 1.1. ILRI.
- Ramos, T.B., Simionesei, L., Jauch, E., Almeida, C., Neves, R., 2017. Modelling soil water and maize growth dynamics influenced by shallow groundwater conditions in the Serraia Valley region, Portugal. *Agric. Water Manage.* 185, 27–42.
- Ren, D., Xu, X., Hao, Y., Huang, G., 2016. Modeling and assessing field irrigation water use in a canal system of Hetao, upper Yellow River basin: application to maize, sunflower and watermelon. *J. Hydrol.* 532, 122–139.
- Rosa, R.D., Paredes, P., Rodrigues, G.C., Alves, I., Fernando, R.M., Pereira, L.S., et al., 2012. Implementing the dual crop coefficient approach in interactive software. 1. Background and computational strategy. *Agric. Water Manag.* 103, 8–24.
- Schaap, M.G., Leij, F.J., van Genuchten, M.T., 2001. Rosetta: a computer program for estimating soil hydraulic parameters with hierarchical pedotransfer functions. *J. Hydrol.* 251 (3–4), 163–176.
- Šimůnek, J., van Genuchten, M.T., Šejna, M., 2005. The HYDRUS-1D Software Package for Simulating the One-Dimensional Movement of Water, Heat, and Multiple Solutes in Variably-Saturated Media, Version 3.0, HYDRUS Software Series 1, Department of Environmental Sciences. University of California Riverside, Riverside, California, USA.
- Šimůnek, J., Hopmans, J.W., 2009. Modeling compensated root water and nutrient uptake. *Ecol. Modell.* 220 (4), 505–521.
- Šimůnek, J., van Genuchten, M.T., Šejna, M., 2012. HYDRUS: model use, calibration, and validation. *ASAE* 55 (4), 1261–1274.
- Šimůnek, J., van Genuchten, M.T., Šejna, M., 2016. Recent developments and applications of the HYDRUS computer software packages. *Vadose Zone J.* 15 (7). <https://doi.org/10.2136/vzj2016.04.0033>.
- Sinclair, T.R., Seligman, N.G., 1996. Crop modeling: from infancy to maturity. *Agron. J.* 88 (5), 698–704.
- Sinclair, T.R., Seligman, N., 2000. Criteria for publishing papers on crop modeling. *Field Crops Res.* 68 (3), 165–172.
- Steduto, P., Hsiao, T.C., Raes, D., Fereres, E., 2009. AquaCrop-The FAO crop model to simulate yield response to water: I. Concepts and underlying principles. *Agron. J.* 101 (3), 426–437.
- Stockle, C.O., Williams, J.R., Rosenberg, N.J., Jones, C.A., 1992. A method for estimating the direct and climatic effects of rising atmospheric carbon dioxide on growth and yield of crops: part I—modification of the EPIC model for climate change analysis. *Agric. Syst.* 38 (3), 225–238.
- Therond, O., Hengsdijk, H., Casellas, E., Wallach, D., Adam, M., Belhouchette, H., et al., 2011. Using a cropping system model at regional scale: low-data approaches for crop management information and model calibration. *Agric. Ecosyst. Environ.* 142 (1–2), 85–94.
- van Dam, J.C., Huygen, J., Wesseling, J.G., Feddes, R.A., Kabat, P., van Walsum, P.E.V., et al., 1997. Theory of SWAP Version 2.0. Simulation of Water Flow, Solute Transport and Plant Growth in the Soil-Water-Atmosphere-Plant Environment. Department of water resources, WAU, Report 71, technical Document 45, DLO Winand Staring Centre-DLO.
- van Diepen, C.A., Wolf, J., van Keulen, H., Rappoldt, C., 1989. WOFOST: a simulation model of crop production. *Soil Use Manag.* 5 (1), 16–24.
- van Genuchten, M.T., 1980. A closed-form equation for predicting the hydraulic conductivity of unsaturated soils. *Soil Sci. Soc. Am. J.* 44 (5), 892–898.
- van Griensven, A., Meixner, T., Grunwald, S., Bishop, T., Diluzio, M., Srinivasan, R., 2006. A global sensitivity analysis tool for the parameters of multi-variable catchment models. *J. Hydrol.* 324 (1–4), 10–23.
- Wang, X., Huang, G., 2008. Evaluation on the irrigation and fertilization management practices under the application of treated sewage water in Beijing, China. *Agric. Water Manage.* 95 (9), 1011–1027.
- Wang, X.P., 2010. Simulation of Water and Nitrogen Use Efficiency and Nitrogen Leaching Risk in a Regional Farmland. PhD Thesis. China agricultural University, Beijing, China (in Chinese).
- Wang, X., Huang, G., Yang, J., Huang, Q., Liu, H., Yu, L., 2015. An assessment of irrigation practices: sprinkler irrigation of winter wheat in the North China Plain. *Agric. Water Manag.* 159, 197–208.
- Williams, J.R., Jones, C.A., Dyke, P.T., 1984. A modeling approach to determining the relationship between erosion and soil productivity. *Trans. ASAE* 1 (27), 129–144.
- Williams, J.R., Jones, C.A., Kiniry, J.R., Spanel, D.A., 1989. The EPIC crop growth model. *Trans. ASAE* 32 (2), 497–511.
- Williams, J.R., Wang, E., Meinardus, A., Harman, W.L., Siemers, M., Atwood, J.D., 2006. EPIC Users Guide v. 0509. Blackland Research and Extension Center, Temple, Texas.
- Wösten, J., Lilly, A., Nemes, A., Le Bas, C., 1999. Development and use of a database of hydraulic properties of European soils. *Geoderma* 90 (3), 169–185.
- Xu, X., Huang, G.H., Qu, Z.Y., Huang, Q.Z., 2011. Regional scale model for simulating soil water flow and solute transport processes-GSWAP. *Trans. CSAE* 27 (7), 58–63 (in Chinese with English abstract).
- Xu, X., Huang, G., Sun, C., Pereira, L.S., Ramos, T.B., Huang, Q., et al., 2013. Assessing the effects of water table depth on water use, soil salinity and wheat yield: searching for a target depth for irrigated areas in the upper Yellow River basin. *Agric. Water Manag.* 125, 46–60.
- Xu, X., Huang, G., Zhan, H., Qu, Z., Huang, Q., 2012a. Integration of SWAP and MODFLOW-2000 for modeling groundwater dynamics in shallow water table areas. *J. Hydrol.* 412–413, 170–181.
- Xu, X., Qu, Z.Y., Huang, G.H., 2012b. Optimization of soil hydraulic and solute transport parameters using genetic algorithms at field scale. *Shuili Xuebao (J. Hydraul. Eng.)* 43 (7), 808–815 (in Chinese with English abstract).
- Xu, X., Sun, C., Qu, Z., Huang, Q., Ramos, T.B., Huang, G., et al., 2015. Groundwater recharge and capillary rise in irrigated areas of the upper Yellow River basin assessed by an agro-hydrological model. *Irrig. Drain.* <https://doi.org/10.1002/ird.1928>.
- Xu, X., Sun, C., Qu, Z., Huang, G., Mohanty, B.P., 2016. Global sensitivity analysis and calibration of parameters for a physically-based agro-hydrological model. *Environ. Model. Softw.* 83, 88–102.
- Yang, J., Reichert, P., Abbaspour, K.C., Xia, J., Yang, H., 2008. Comparing uncertainty analysis techniques for a SWAT application to the Chaohe Basin in China. *J. Hydrol.* 358 (1), 1–23.
- Zhao, G., Bryan, B.A., Song, X., 2014. Sensitivity and uncertainty analysis of the APSIM-wheat model: interactions between cultivar, environmental, and management parameters. *Ecol. Modell.* 279, 1–11.